Dye molecules on titanium dioxide surface: cluster and periodic surface models

Ville Mäkinen

UNIVERSITY OF JYVÄSKYLÄ
DEPARTMENT OF PHYSICS

Master's thesis
Supervisors: Michael Walter, Hannu Häkkinen
December 1, 2008

ABSTRACT

Dye-sensitized solar cells have been studied actively over decades. They offer a cheaper way to convert sunlight into electricity by replacing the silicon with cheaper titanium dioxide. Due to wider band gap in TiO_2 special dye molecules must be used to sensitize titanium dioxide nanoparticles to visible light.

We have studied the electron interaction of dye molecules and anatase surface via density functional theory. Our motivation is to understand the electron injection process from the dye to the TiO_2 nanoparticles. Then computer simulations could be used to search effective dye molecules for the DSCs.

Our calculations using two dyes and two different surface models show that there are still open questions in interpreting the results. In our calculations the locations of the molecular states relative to the semiconductor bands are not in agreement with the principal idea of the injection process. There is also high exchange-correlation dependence in the results.

Acknowledgements

I would like to thank my supervisor Michael Walter for his excellent guidance and advices, and for supporting words during the writing of this thesis. I am grateful to Hannu Häkkinen for giving interesting material physics courses and introducing me to the condensed matter physics. Also my office mates at Holvi deserve compliments for providing an enjoyable working environment.

Jyväskylä, June 2008
Ville Mäkinen

Contents

ABSTRACT i

Acknowledgements ii

1 Introduction 1
1.1 The basic structure of the cell . . . 2
1.2 The principles of operation . . . 2
1.3 Efficiency . . . 3

2 Theory 4
2.1 Born-Oppenheimer approximation . . . 4
2.2 Density functional theory . . . 5
2.3 Kohn-Sham method . . . 5
2.4 Functionals . . . 7
2.4.1 The local density approximation . . . 7
2.4.2 Generalized gradient approximation . . . 8
2.4.3 The PBE functional . . . 8
2.4.4 The exact exchange . . . 9
2.4.5 The PBE0 functional . . . 9
2.4.6 PBE+U method . . . 10
2.5 Boundary conditions in simulations . . . 10
2.6 The band structure and density of states . . . 12
2.7 Computational methods . . . 12
2.7.1 Pseudo-potential approach . . . 13
2.7.2 Projector augmented-wave method (PAW) . . . 13
2.8 Real-space implementation of the PAW method . . . 14
2.9 Projected density of states (PDOS) . . . 15
2.10 Charge analysis . . . 15

3 Calculations 17
3.1 Dye molecules in gas phase . . . 17
3.2 Bulk TiO_2 (anatase) . . . 19
3.3 Anatase (101) surface . . . 20
3.4 Periodic surface models . . . 22
3.5 Cluster model . . . 26
3.6 Cluster model with nko_001 . . . 29
3.7 Periodic model with nko_001 . . . 31
3.8 Periodic model with perylene . . . 34

4 Conclusions 36

References 41

A Functional derivatives 42

B Bloch's theorem 43

1 Introduction

The dye-sensitized solar cells (DSC), or Grätzel cells, are a new and promising type of solar cells. They are built from cheaper materials than the silicon-based solar cells, which basically need pure silicon with no impurities to work efficiently.

A silicon-based solar cell contains two types of silicon material. One metal electrode is layered with p-doped silicon and the other with n-doped silicon. These are in contact and at this contact surface (called the p-n-junction) an electric field emerges. In silicon the band gap is so small that light can excite an electron from the valence band to conduction band, leaving an empty electron vacancy (a hole) in the valence band. The electric field then separates these charge carrier and forces them to move in opposite directions, thus creating current when the circuit is closed.[1,2]

In Grätzel cells the silicon is replaced with another semiconductor. In general, the band gap of a semiconductor is too wide for visible light to excite electrons over the gap. However, semiconductors can be sensitized to visible light by attaching suitable molecules onto their surface. This was discovered over hundred year ago but the study of the dye-sensitized solar cells really began in 1960s.[3] Since then they have been under active study. Titanium dioxide has become the most popular semiconductor to be used in the DSCs.[4] In this work we study the interaction of certain dye molecules and TiO_2 surface from theoretical point of view.

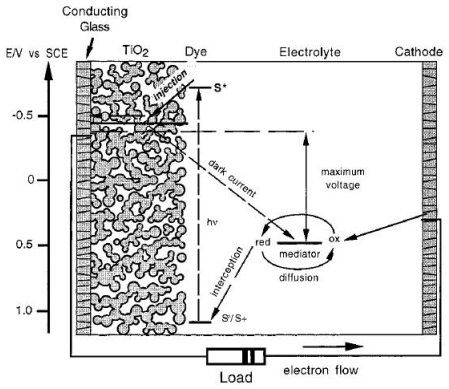

Figure 1 *– The schematic structure of a dye-sensitized solar cell. The two electrodes are located on the sides of the cell. The other electrode is covered with porous semiconductor material and the cell is filled with elecrolyte. Picture taken from ref. 3.*

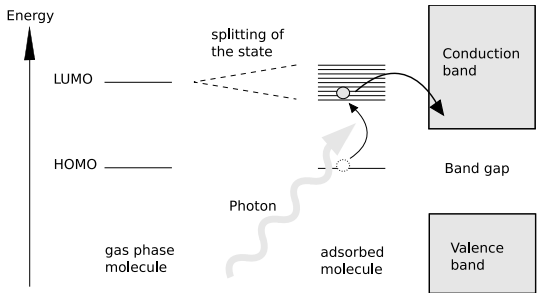

Figure 2 *– Left: The molecule HOMO and LUMO in gas phase. Right: The molecule HOMO and broadened LUMO when it's adsorbed on the surface of the semiconductor.*

1.1 The basic structure of the cell

The basic idea of a dye-sensitized solar cell is well described in ref. 3. A general structure is shown in Figure 1. The cell consists of two electrodes placed in a container. One electrode is covered with a layer of porous semiconductor material. Porous material has a lot of holes and cavities making its surface-to-volume ratio huge. This can be achieved by sintering TiO_2 nanoparticles together. It is important that the particles are in good contact with each other to get efficient conductance to the electrode from every point of the porous layer.

The dye molecules are then attached onto the surface of this material. Because of the porous structure the amount of adsorbed dye molecules is greatly increased compared to the flat surface. Finally the container is filled with electrolyte which connects the porous TiO_2 layer to the other electrode and closes the circuit.

1.2 The principles of operation

The situation in the dye-sensitized solar cell is different than in the plain silicon environment, where the electron is spatially always located in the semiconductor. In the simplest picture the photoexcitation process goes as presented in the Figure 2. The dye molecule absorbs a photon and gives its energy to the electron located on the highest occupied molecular orbital (HOMO). The electron is subsequently lifted to the lowest unoccupied molecular orbital (LUMO). Finally the electron is injected from the LUMO to the conduction band (CB). The molecule is then restored to the ground state by accepting an electron from the electrolyte.

The rate of the injection process from the LUMO to the CB is affected

by their mutual interaction, which is the main target of this study. The interaction is seen as the LUMO splitting into several states. The stronger the interaction is the more the LUMO is broadened and the faster the injection process is. The interaction is stronger where the density of states of the conduction band is higher. In the single particle picture the density of states $g_{3D}(E)$ of a three dimensional bulk material as the function of energy is approximated by

$$g_{3D}(E) \propto \sqrt{E}, \tag{1}$$

i.e, it increases as the energy increases (see ref. 5, chapter 5.1). This indicates that the deeper (or higher) the LUMO is located in the conduction band, the stronger the interaction is. However, one must also notice that after the electron is injected into the semiconductor, it will fall to the lowest possible state, in this case, to edge of the CB, losing some of it's energy to the nanocrystal. This loss of energy decreases the voltage between the two electrodes, and thus, the maximum output power the cell can produce. Therefore it is not trivial to say what would be the optimal placement of the LUMO relative to the CB.

In this work we decided to study two different dye molecules. One is used in experiments by Kitamura et al. [6] and has been able to produce current in the DSC. The other is studied via computational methods by Persson et al. [7]. According to their results also this molecule should work efficiently in the DSC.

In this approach we only study the adiabatic electron injection process, i.e, tunneling from the LUMO to the CB. We are ignoring the effects of the movement of the atoms since the injection process is thought to be extremely rapid event. If the molecular dynamics were taken into account, there would also be other mechanisms that affect the electron injection process. Duncan et al. [8] suggested that the electron transfer process can happen, in addition to adiabatic transfer, with non-adiabatic quantum-mechanical tunneling mechanism. This process becomes more important if the LUMO-CB -interaction is not strong.

1.3 Efficiency

After the electron has been excited to the LUMO state it is instantaneously injected to the porous semiconductor, assuming that the rate of the injection process is fast enough. However, not all the excited electrons that are injected to the conduction band reach the electrode. The path the electrons have to travel is relatively long, due to the porous structure of the titanium dioxide. During the travel they might come across with another

dye molecule that has just lost an electron due to photoexcitation and recombinate with it. The nanoparticles also have crystal defects due to impurities and surface effects. These give rise to energy distortions to the band structure and may create so-called surface traps (energy holes) to the semiconductor where the electron might get stuck. The electrolyte in the cell is also present in the cavities of the porous titanium dioxide, and a positive ion of the electrolyte may capture a traveling electron.[3,9,10]

It's clear that the thicker the porous layer on the electrode is the harder it is for a photoexcited electron to reach the electrode. On the other hand the number of adsorbed dye molecules is proportional to the thickness of the layer. The optimal thickess of the layer is therefore one of the variables that must be worked out when manufacturing these kind of solar cells.

2 Theory

2.1 Born-Oppenheimer approximation

The atom nuclei are massive compared to the electrons. In the Born-Oppenheimer approximation[11,12] it is assumed that the electrons react instantaneously to the movement of the nuclei. In other words, for any given atom configuration the electrons are always located in the energetically lowest possible configuration. Another way to explain this approximation is that since the movement of the electrons is rapid compared to the movement of the nuclei, they "see" the change of the locations of the nuclei as an adiabatic change in the system.

With these approximations the total energy of the system is

$$E_{total} = \sum_i \frac{1}{2} m_i \dot{\vec{r}_i}^{\,2} + \sum_i \sum_{j>i} \frac{Z_i Z_j}{|\vec{r}_i - \vec{r}_j|} + E_{elec}\left(\{\vec{r}_i\}\right) \ , \tag{2}$$

where $\vec{r}_i$ is the position, $\dot{\vec{r}_i}$ the velocity, m_i the mass and Z_i the charge of i:th ion. The first term describes the classical kinetic energy of the ions and the second the Coulombic interaction of the ions. The index of summation at second term is $i > j$ to count each ion-ion interaction only once and to exclude self-interaction. The third term is the total energy of the electron gas in current ion configuration (the $\{\vec{r}_i\}$ stands for a list of all positions of the ions).

The first and the second term are more or less easy to calculate. The total energy of the electron gas is calculated via the density functional theory (DFT).

2.2 Density functional theory

Traditionally methods for calculating the energy of the electron gas are based on using many-electron wave functions. For N electrons, one has 3N variables to work out[1].

In the density functional theory the electron gas is described using the electron density as a variable. The theory is based on the fact that any two potentials $V_{ext}(\vec{r})$ and $V'_{ext}(\vec{r})$ that differ more than by a constant define different ground state electron gas densities. This means that the electon density $n(\vec{r})$ fully determines the ground state of the electron gas. Therefore one can write the ground state energy as a functional of the electron gas density. This was shown by Hohenberg and Kohn in 1964 in ref. 13. The electronic energy of the system can be expressed in form

$$E[n](\vec{r}) = F[n](\vec{r}) + \int n(\vec{r})V_{ext}(\vec{r})d\vec{r}, \tag{3}$$

where the first term is yet undefinded energy functional and the second the potential energy of the electrons moving in the external potential.

2.3 Kohn-Sham method

Soon after the paper from Hohenberg and Kohn a practical way to solve the density of the electron gas for the ground state was introduced by Kohn and Sham[14] which is briefly described in the following.

The basic idea is that N interacting electrons in a potential V_{ext} created by the ions are replaced with N non-interacting electrons in an effective potential V_{eff}. The effective potential must produce the same electron density of non-interacting electrons as in the original system of real electrons. This kind of potential is not always found and in that case the theory needs to be formulated in a slightly different way (see ref. 12, v- and N-representability).

The non-interacting electrons can be described with a Slater determinant of one-electron wave functions. From these WFs one can calculate the kinetic energy of the non-interacting electrons. The undefined energy functional $F[n](\vec{r})$ in equation (3) is therefore decomposed into three parts:

$$F[n](\vec{r}) = T_S[n](\vec{r}) + \frac{e^2}{2}\iint \frac{n(\vec{r})n(\vec{r}\,')}{|\vec{r}\,' - \vec{r}|}d\vec{r}d\vec{r}\,' + E_{XC}[n](\vec{r})\,, \tag{4}$$

[1]More precisely 3N-5, since the position and the angular momentums of one atom can be fixed if there is no external potential.

where the first term is the kinetic energy of the non-interacting electrons the second the classical electron-electron Coulomb interaction. The final term is called the exchange-correlation (XC) term. It can be defined as an error between the "true" energy functional and the rest of the $F[n](\vec{r})$ defined in equation (4). The true form of this functional is unknown and many approximations have been developed. These are discussed more in section 2.4.

There are some conditions the density must fulfill. First, the number of electrons must not change during the variation so we have

$$\delta n = \int \frac{\delta n}{\delta n(\vec{r})} \delta n(\vec{r}) d\vec{r} = \int \delta n(\vec{r}) d\vec{r} = 0 \tag{5}$$

Second, for the ground state the energy defined in equation (3) must be minimum with respect to the variation of $n(\vec{r})$, so

$$\begin{aligned} \delta E &= \int \frac{\delta E}{\delta n(\vec{r})} \delta n(\vec{r}) d\vec{r} \\ &= \int \delta n(\vec{r}) \left\{ \frac{\delta T_S[n]}{\delta n(\vec{r})} + V(\vec{r}) + \mu_{XC}[n](\vec{r}) \right\} d\vec{r} \\ &= \int \delta n(\vec{r}) \left\{ \frac{\delta T_S[n]}{\delta n(\vec{r})} + V_{eff}(\vec{r}) \right\} d\vec{r} = 0 \,, \end{aligned} \tag{6}$$

where

$$V(\vec{r}) = V_{ext}(\vec{r}) + \int \frac{n(\vec{r}\,')}{|\vec{r} - \vec{r}\,'|} d\vec{r}\,' \quad \text{and} \quad \mu_{XC}[n](\vec{r}) = \frac{\delta E_{XC}[n]}{\delta n(\vec{r})} \tag{7}$$

(see Appendix A for the calculation of the functional derivatives).

Because we are dealing with non-interacting electrons, we can solve the electron density for N electrons by solving N one-particle Schrödinger equations

$$\left(-\frac{1}{2}\nabla^2 + [V(\vec{r}) + \mu_{XC}[n](\vec{r})] \right) \psi_i(\vec{r}) = \epsilon_i \psi(\vec{r}) \tag{8}$$

and setting

$$n(\vec{r}) = \sum_{i=1}^{N} |\psi_i(\vec{r})|^2 \,. \tag{9}$$

Finally the total energy of the ground state is given by

$$E = \sum_i \epsilon_i - \frac{1}{2} \iint \frac{n(\vec{r})n(\vec{r}\,')}{|\vec{r} - \vec{r}\,'|} d\vec{r} d\vec{r}\,' + E_{XC}[n] - \int n(\vec{r})\mu_{XC}[n](\vec{r})d\vec{r}, \quad (10)$$

where

$$\sum_i \epsilon_i = \sum_i \langle \psi_i | - \nabla^2 + V_{eff} | \psi_i \rangle = T_s[n] + \int n(\vec{r}) V_{eff}(\vec{r}) d\vec{r} \quad (11)$$

There is no general solution to solve equations (7)-(9) exactly, one reason being that the E_{XC} is unknown. Instead they are solved self-consistently using an iterative method. First some initial density $n(\vec{r})$ is used to solve the potentials $V(\vec{r})$ and $\mu_{XC}(\vec{r})$. Then they are used in order to solve new wave functions with (8) and new density with (9). This is repeated until the change of the density between iterations is smaller than a prescribed limit.

It should be emphasized that the basic density functional theory is only able to find and describe the ground state of the system. When the Kohn-Sham method is applied one gets a set of single-particle states. These states should not be blindly interpreted as the real electron states because they are the solutions to the system of fictious non-interacting electrons. However, they give some information of the system, for example the energy of the highest occupied KS-state corresponds to the chemical potential.[12] It is a common approximation to use these states to calculate the density of states of the system under study. The excited states are problematic because they usually become very dependent of the exchange-correlation energy used.

There are also other methods to calculate the excited state properties. One method to calculate the excited state of the system is called the time-dependent density-functional theory (TDDFT) (see for example ref. 15 for short introduction).

2.4 Functionals

2.4.1 The local density approximation

The exchange-correlation (XC) functional contains all the errors that are made when calculating the properties of the real system using the non-interacting one. Kohn and Sham used the local density approximation (LDA) in their derivation,[14]

$$E_{XC}^{LDA}[n] = \int n(\vec{r})\epsilon_{XC}[n](\vec{r})d\vec{r}, \quad (12)$$

where the $\epsilon_{XC}[n]$ is the exchange-correlation energy density of uniform electron gas. The $\epsilon_{XC}[n](\vec{r})$ has been constructed from Monte Carlo simulations.[16] In principle the LDA should only work when the density of the electron gas is almost homogeneous. It has been, however, found to give very good results even when the density of electron gas varies rapidly.

2.4.2 Generalized gradient approximation

To take into account the changes in the density of the electron gas the gradient of the density must be included somehow to the XC energy. In that case the approximation is called the generalized gradient approximation (GGA). It has the general form

$$E_{XC}^{GGA}[n] = \int f(n(\vec{r}), \nabla n(\vec{r}))d^3\vec{r}\,. \tag{13}$$

Many different kinds of functionals have been developed, and there is no easy way to tell which is the best. Some work well in some situations and fail in others. Some rely on fitted parameters to experimental data while others have been derived purely from the theoretical basis.

2.4.3 The PBE functional

The PBE XC-functional was developed by Perdew, Burke and Ernzerhof in 1996[17] to correct the problems with another functional, PW91.[18] PW91 was developed by Perdew and Wang in 1991. It needs corrections because it introduces unphysical effects with both small and large density gradients.

The PBE enchange-correlation functional is

$$\begin{aligned} E_{XC}^{PBE}[n] &= \int n(\vec{r})\epsilon_{XC}[n](\vec{r})F_{XC}(r_s,\zeta,s)d\vec{r}, \\ F_{XC} &= 1+\kappa-\kappa/(1+\frac{\mu s^2}{\kappa}), \end{aligned} \tag{14}$$

where r_s is the local Seitz radius ($n = \frac{3}{4}\pi r_s^3$), ζ is the spin polarisation ($\zeta = (n\uparrow - n\downarrow)/n$) and s is a dimensionless density gradient, and κ and μ are numerical constants. The functional is derived so that it satisfies as many as possible of the known features of the XC-energy which are physically important, which was found out not to be the case with PW91. Also, the PBE is derived purely from theoretical basis, i.e., no experimental data is used to fit any of the parameters (other than those in the ϵ_{XC}). The PBE functional usually gives better results compared to the LDA.

2.4.4 The exact exchange

The Coulomb term in equation (4) (the double integral) gives contribution to the total energy even when dealing with only one electron (hydrogen atom). This self-interaction is obviously unphysical.

In Hartree-Fock approximation[12] the N-electron wave function is described as a Slater determinant using the single-particle states ψ_i. In the ground state N lowest states are occupied and the wave function is

$$\Psi(\vec{r}_1, ..., \vec{r}_N) = \frac{1}{\sqrt{N}} \begin{vmatrix} \psi_1(\vec{r}_1) & \dots & \psi_1(\vec{r}_N) \\ \vdots & \ddots & \vdots \\ \psi_N(\vec{r}_1) & \dots & \psi_N(\vec{r}_N) \end{vmatrix}. \tag{15}$$

Calculating the expectation value of the Hamiltonian gives the kinetic energy, external potential energy and the Coulombic electron-electron interaction energy, but also an additional negative term, called the exchange term, giving the total energy

$$\begin{aligned} E^{HF} = \langle \Psi | \hat{H} | \Psi \rangle = T_s + \int n(\vec{r}) V_{ext}(\vec{r}) d\vec{r} + \frac{1}{2} \iint \frac{n(\vec{r}) n(\vec{r}')}{|\vec{r} - \vec{r}'|} d\vec{r} d\vec{r}' \\ \underbrace{-\frac{1}{2} \sum_{i,j} \iint \frac{\psi_i^*(\vec{r}) \psi_i(\vec{r}') \psi_j^*(\vec{r}') \psi_j(\vec{r})}{|\vec{r} - \vec{r}'|} d\vec{r} d\vec{r}'}_{= E_X^{HF}}, \end{aligned} \tag{16}$$

where the indices i and j go over all the states and since the states are occupied we have also used

$$n(\vec{r}) = \sum_i |\psi_i(\vec{r})|^2 . \tag{17}$$

For example in the case of an isolated hydrogen atom the exchange term fully cancels the self-interaction of the single electron. This is the rationale for mixing the exact exchange to the XC-functionals.[19]

2.4.5 The PBE0 functional

The PBE0 is one functional that has exact exchange mixed in it. It is derived from the PBE and the zero means that there are no additional adjustable

parameters compared to the PBE.[20]

$$E_{XC}^{PBE0} = E_{XC}^{PBE} + \frac{1}{4}\left(E_X^{HF} - E_X^{PBE}\right) \tag{18}$$

The constant $\frac{1}{4}$ is derived from the fourth-order perturbation theory and the E_X^{HF} is the exchange energy of the Hartree-Fock approximation. Unfortunate aspect of functionals that have exact exchange mixed in them is that the number of integrations in the exchange term is proportional to the number of states squared. This functional is suitable for small molecules but with large systems the calculations become more demanding.

2.4.6 PBE+U method

As mentioned before, the LDA has proven to be a good approximation for many systems, for example for large molecules and solids. According to Anisimov et al. [21] the failing of the LDA can be seen clearly with strongly correlated materials. Such materials usually contain partially filled d of f shell (for example transitions metals and rare earth metals). In the LDA+U method the electrons are separated into two groups, the localized d (or f) electrons and delocalized s and p electrons. The s and p electron are treated with normal LDA approximation but for the d (and f) electrons the Coulomb interaction must be taken into account, with an energy term of the form

$$E_{corr} = \frac{1}{2}U\sum_{i\neq j} n_i n_j, \tag{19}$$

where n_i is the d (or f) orbital occupation numbers and $N = \sum_i n_i$ is the total number of d-electrons. It is then assumed that the Coulomb energy of d-d interactions as a function of the number of d-electrons given by the LDA is a good approximation, so this energy is subtracted from the LDA XC-functional and the orbital-dependent term (19) is added. The exchange-correlation functional in this method is

$$E[n] = E_{PBE} - \frac{UN(N-1)}{2} + \frac{1}{2}U\sum_{i\neq j} n_i n_j \tag{20}$$

The orbital energies of the d-orbitals are then given by

$$\epsilon_i = \frac{\partial E[n]}{\partial n_i} = \epsilon_i^{PBE} + U\left(\frac{1}{2} - n_i\right). \tag{21}$$

2.5 Boundary conditions in simulations

Performing DFT calculations for small isolated molecules is relatively simple. One constructs the molecule and places it in a simulation cell. The boundary conditions are set so that the wave functions (and their derivatives) must vanish at the boundaries of the simulation cell. This is why there must be some empty space between the atoms and the walls of the simulation box. Usually a few Å is enough.

The anatase nanoparticles in the DSCs contain so huge number of atoms that simulating the whole particle is not computationally possible and not even reasonable. If the system has some kind of lattice structure that can be built from a primitive unit cell, the potential created by the nuclei is periodic,

$$V(\vec{r} + \vec{R}) = V(\vec{r}), \tag{22}$$

where $\vec{R} = N_a\vec{a} + N_b\vec{b} + N_c\vec{c}$ is a translation vector in the real space lattice (the vectors $\vec{a}$, $\vec{b}$ and $\vec{c}$ define the unit cell and the multipliers N_i are integers). The periodicity is of course broken at the surfaces of the particle. In our case the TiO_2 nanoparticles are so huge compared to the dye molecules that we can as well treat the nanoparticles as infinite surfaces. For this we can introduce periodic boundary conditions. We can choose some unit cell that produces the periodic potential and use it as the simulation box. In this approach there is no need to put extra empty space in the box. The WFs do not have to vanish at the boundaries. Instead they must be solutions for the Schrödinger equation with the periodic potential. The simplest form of this kind of WF is

$$\Psi(\vec{r} + \vec{R}) = \Psi(\vec{r}). \tag{23}$$

(see Figure 3). Bloch's theorem (see ref. 5) allows us to work with bigger set

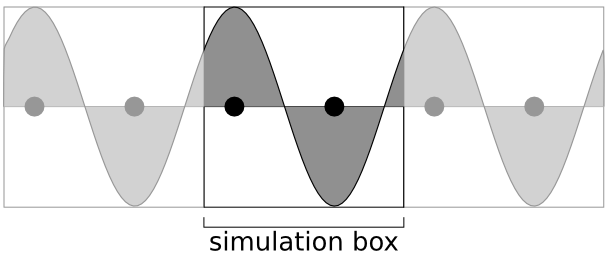

Figure 3 *– The periodic boundary conditions applied in one-dimensional case. The wave functions do not have to vanish at the boundaries, but match the values at the opposite side of the cell.*

of wave functions. It states that the wave functions in the periodic potential are of the form

$$\Psi_{\vec{k}}(\vec{r}) = e^{i\vec{k}\cdot\vec{r}} u_{\vec{k}}(\vec{r}), \tag{24}$$

where $u_{\vec{k}}(\vec{r})$ is a real-valued function that has the same periodicity as the potential and it is modulated by a plane-wave. The Bloch boundary conditions are then

$$\Psi_{\vec{k}}(\vec{r} + \vec{R}) = e^{i\vec{k}\cdot\vec{R}} \Psi_{\vec{k}}(\vec{r}). \tag{25}$$

One Bloch wave is visualized in Appendix B.

2.6 The band structure and density of states

The Bloch wave functions are fully periodic in the reciprocal lattice,

$$\Psi_{\vec{k}+\vec{G}}(\vec{r}) = \Psi_{\vec{k}}(\vec{r}), \tag{26}$$

where the vector $\vec{G}$ is a similar lattice-vector in the reciprocal space as the $\vec{R}$ is in the real space in equation (22). The primitive unit cell in the reciprocal space is called the 1st Brillouin zone. From the periodicity in the reciprocal space it follows that all the information of the Bloch wave function can be calculated using the $\vec{k}$-vectors inside the 1st BZ.

The band structure can be calculated so that one moves along some path in the 1st BZ and plots the energy of each Bloch state as a function of $\vec{k}$. Obviously there are infinite number of different paths. Usually the path is chosen to be a number of lines that start from and end to some symmetry point in the 1st BZ. The trivial point is $\vec{k} = (0, 0, 0)$, denoted as the Γ-point. The definition of other symmetry points is ambiguous since they depend on the type of the reciprocal lattice. One calculated band structure is shown in Figure 4.

The density of states (DOS) is obtained when the band structure is projected to the energy axis. In principle all the k-points should be included when calulating the DOS. In practise a discrete number of points are chosen from the 1st BZ and the energies of the Bloch states are calculated at these points. In principle increasing the number of k-points results in more accurate DOS.

2.7 Computational methods

Accurate expression of the electron wave functions in many-atom systems is difficult due to the fact that the shapes of the wave functions are different in

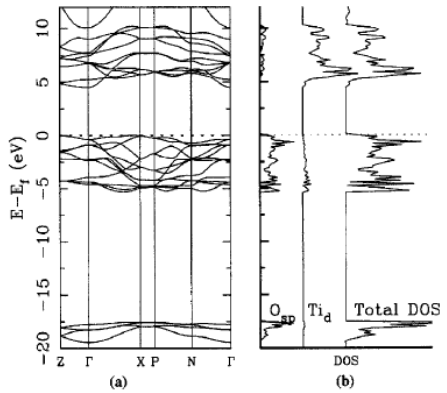

Figure 4 *– The calculated band structure for anatase with PBE0. Picture taken from ref 22.*

different locations of the system. Between the atoms the wave functions can be very smooth, whereas near the atoms there are always large oscillations due to fact that the wave functions must be orthogonal to each other and the core states of the nuclei. This means that if one wants to use only, say, plane waves to describe the wave functions, the set of the used plane waves must be very large. This leads immediately to problems as the computational demands grow with the number of used plane-waves.

2.7.1 Pseudo-potential approach

Usually the wave functions near the core are not chemically interesting. In the pseudo-potential method some radius is chosen so that inside the sphere of that radius the real oscillating wave functions are replaced by smooth fixed pseudo-wave functions. The pseudo-wave functions must produce the same charge as the real wave functions. On the surface of the sphere the real and pseudo WFs and their derivatives must be continuous and outside the sphere the WFs are the same. This approach is a rough approximation but when calculating for example the dissociation energy of a H_2 molecule the wave functions near the cores usually do not change substantially and because the same approximation is done on the both molecule and isolated atoms the errors arising from the pseudo-potential approximation cancels out.

2.7.2 Projector augmented-wave method (PAW)

The projector augmented-wave method was developed by Blöchl [23]. The principal idea of the projector augmentation-wave method is similar to the pseudo-potential approach. The spheres around the atoms are called augmentation spheres in the PAW formalism. In the PAW method for each electron there is so-called pseudo (PS) wave-function $|\widetilde{\Psi}\rangle$ that is defined everywhere in space. Outside the spheres the PS wave function is the same as the real all-electron (AE) wave function $|\Psi\rangle$. Inside the augmentation spheres the corrections from the core electrons to the PS wave function are defined. These are called partial PS and AE wave functions, $|\widetilde{\phi}_a\rangle$ and $|\phi_a\rangle$ respectively. The index a refers to a specific augmentation sphere. The real wave function is then given as

$$|\Psi\rangle = |\widetilde{\Psi}\rangle + \sum_a c_a \left(|\phi^a\rangle - |\widetilde{\phi}^a\rangle \right). \tag{27}$$

2.8 Real-space implementation of the PAW method

Mortensen et al. [24] derived a real-space implementation of the PAW method, called GPAW.[25] GPAW is a DFT code where the wave functions (and densities) are stored in a real-space grid. In the PAW method the memory requirements can be cut by the use of different grids. The smooth part of the wave function can be described accurately enough on a coarse uniform grid. The real and pseudo partial waves are described using denser radial grids inside the augmentation spheres.

The partial AE wave functions are taken from calculations of isolated atoms and they are of the form

$$|\phi^a\rangle = \sum_i |\phi_i^a\rangle \,, \tag{28}$$

where

$$\phi_i^a(\vec{r}) = \phi_{nl}^a(r) Y_{lm}(\Omega). \tag{29}$$

This gives the all-electron wave function

$$|\Psi\rangle = |\widetilde{\Psi}\rangle + \sum_a \sum_i c_i^a \left(|\phi_i^a\rangle - |\widetilde{\phi}_i^a\rangle \right). \tag{30}$$

The good aspect of the real-space approach is that the parallelization of the calculations is easier than for example when dealing with plane

waves. The real-space grid can be divided into several domains and each processor can calculate large proportion of needed calculation without communicating with other processors. For example the derivatives of the wave functions that are needed in many cases (for example when evaluating the value of the PBE functional) can be calculated using the adjacent grid points, and therefore communication is only needed when dealing with grid points near the domain edges.

2.9 Projected density of states (PDOS)

Density of states is needed in order to study the electron injection from the dye to the semiconductor. In the Kohn-Sham formulation of the DFT we get the density of the KS states which we use to approximate the real DOS.

When dealing with systems that have clearly different domains in real space (TiO_2-surface and dye molecule) it is necessary to know where the states are located spatially. This can approximated in many ways. We decided to use projected density of states approach. The initial guess for the wave functions are constructed from the solutions of the isolated atoms. During the calculation the states change and mix and the coefficients are not the same as in the beginning. We use these coefficients as a weight factor of a state over a specific atom.

2.10 Charge analysis

In the DFT one of the physical quantities one gets out of the calculations is the electron density. One way to analyse the system is to compare the electron density over different atoms. The size of the atom is not precisely defined quantity and there are many ways to define the region which belongs to a specific atom. Therefore, if one calculates the charge for a single atom in many-atom system (for example in a bulk material or molecule) the number should be always treated as some kind of approximation.

In the Wigner-Seitz approximation all the atoms are treated equivalently and the space is divided into regions as in the Wigner-Seitz cells in the reciprocal lattice (see Figure 5). This would be completely acceptable method if all the atoms were similar (for example in solid iron), but we are studying titanium dioxide where we have different kinds of atoms, titanium and oxygen atoms. The atomic radius of the titanium, depending which definition is used, is over two times larger than the oxygen radius[26] so the Wigner-Seitz way of dividing space into regions would feel a little crude.

Physically more intuitive method to analyze charges of atoms in molecules was developed by Richard Bader (see ref. 12). The idea is to separate the electron density by using special cutting surfaces. In three dimensions the definition of the cutting surface is that on the point on the surface the gradient of the density has no component normal to that surface.[27] One-dimensional example is shown in Figure 6.

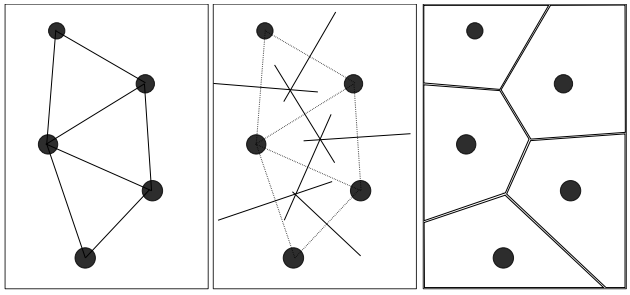

Figure 5 *– The procedure to define the Wigner-Seitz cell. First the atoms are connected with straigh lines. Then the lines are cut from the center point with orthogonal lines, and these lines are used to divide the space.*

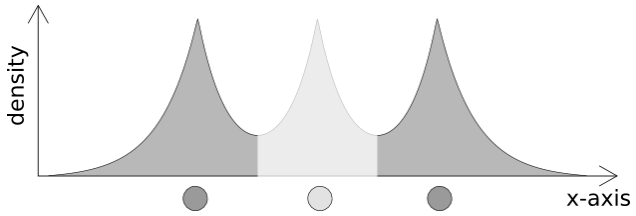

Figure 6 *– Schematic electron density in one dimension. The different colors represent the regions given by the Bader analysis. The charge for a specific atom is obtained by intergrating the electron density in the corresponding region.*

3 Calculations

We studied the interaction between the dye molecules and titanium dioxide using the methods described in previous section. The densities of states is calculated from the dye molecules in vacuum, from the TIO_2 surface models and finally from the combined systems. The results are compared to other studies and to the general idea of the electron injection in the DSCs.

3.1 Dye molecules in gas phase

In this study we decided to use two different dye molecules, called nko_001 and perylene. The dye molecules are shown in Figure 7. Nko_001 has been used in experiments and efficiency of over 5% has been achieved in DSC with this dye (molecule 2a in ref. 6). Perylene has been studied from theoretical point of view using similar methods we are using.[7] Both molecules have a COOH-group attached from where it can be attached to the TiO_2 surface. We have previously calculated the DOS for these molecules in vacuum using Born-Oppenheimer Molecular Dynamics (BOMD) approximation with the PBE exchange-correlation functional and pseudo-potentials devised by Troullier and Martins.[28]

The results from both calculations are shown in Figure 8. Only the KS orbital energies are plotted and the Fermi energy is shifted to zero. The results are consistent with each other, especially the HOMO-LUMO gap. The biggest difference in these calculations was that the core regions of the WFs are described accurately in the GPAW calculations. This indicates that the oscillating parts of WFs near the atom cores do not affect the results substantially in these systems.

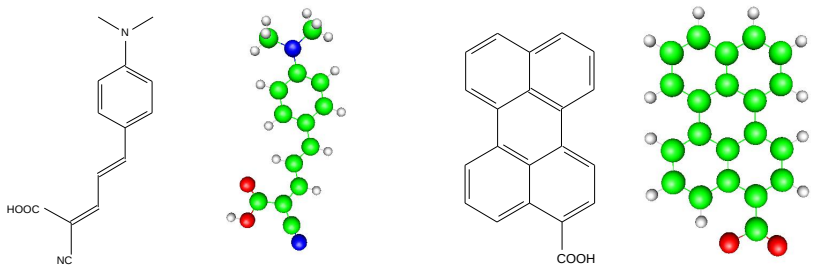

(a) nko_001 **(b)** perylene

Figure 7 *– Chemical structures and visualizations of the studied dye molecules. The small atoms in the visualizations are hydrogen atoms.*

We calculated the density of states for these molecules in vacuum using

both PBE and PBE0 functionals. We fold the results with Gaussian peaks to make them easier to read and shift the HOMO-LUMO gap (or band gap in the case of TiO_2) to zero energy. The DOSs for the dyes are shown in Figure 9. Compared to the PBE functional the PBE0 results to wider HOMO-LUMO gaps. Otherwise the shapes of the DOSs are similar. The HOMO and the LUMO are isolated peaks in both Figures with both XC functionals.

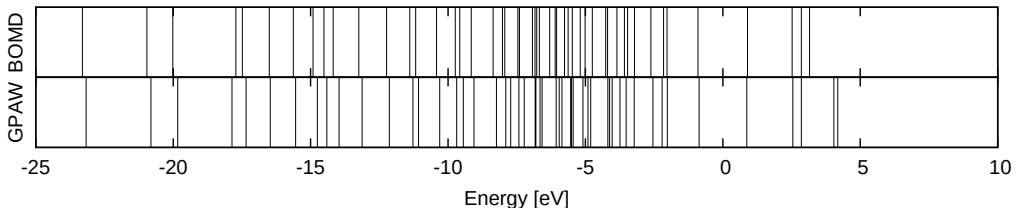

(a) nko_001

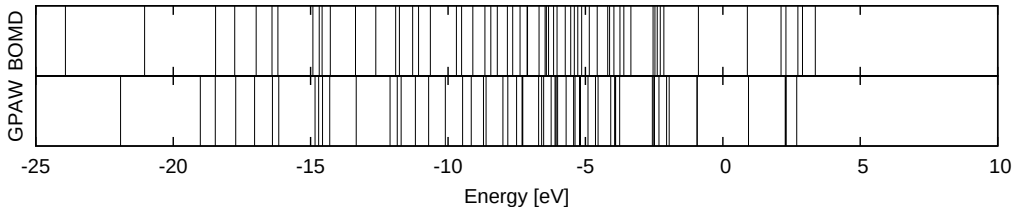

(b) perylene

Figure 8 *– The Kohn-Sham states of the dye molecules in vacuum calculated with the BOMD and the GPAW, both with the PBE functional.*

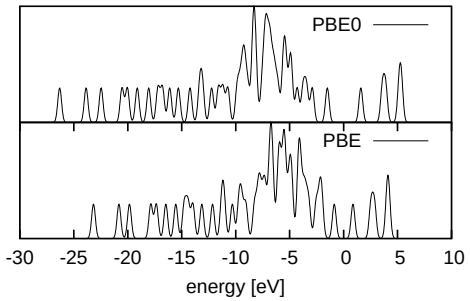

(a) nko_001

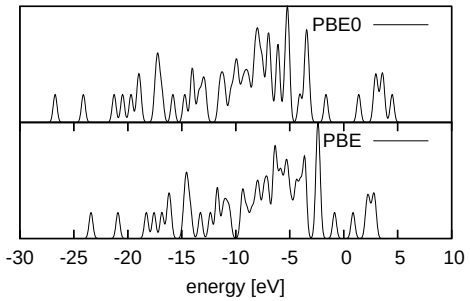

(b) perylene

Figure 9 *– The density of states of the studied dye molecules in vacuum with two exchance-correlation functionals*

3.2 Bulk TiO_2 (anatase)

One way to manufacture porous titanium dioxide is to sinter together TiO_2 particles whose diameter is a few nanometers.[3] Titanium dioxide has three common crystal forms: anatase, rutile and brookite. The dominating structure of titanium dioxide nanoparticles is believed to be anatase.[29] The bulk anatase is a periodic structure which means that there exists an unit cell that can be multiplied to form an anatase particle of an arbitrary size. The size of the unit cell is defined by the periodicity of the structure. In anatase the size of the cell is roughly 9.5 Å$\times 3.8$ Å$\times 3.8$ Å.[30] This is shown in Figure 10. We calculated the DOS for the bulk anatase by using the unit cell of the anatase and applying periodic boundary conditions to all directions. The DOS was calculated with four different number of $\vec{k}$-points. The results from these calculations are shown in Figure 11, where the naming means that there is the shown number of $\vec{k}$-points in each direction where the periodic boundary condition are applied (for example in this case the k2 means that there are 2x2x2=8 $\vec{k}$-points included). The number of $\vec{k}$-points affects the DOSs in a way that whenever the Γ-point is included there is a little bump at the edge of the conduction band (at 1 eV). This is also seen in other studies[22,31] where the band structure of anatase is calculated. Both studies show that there is an indirect gap in anatase from near the X-point to the Γ-point. The valence band is relatively smooth but the conduction band has large hole at the Γ-point and that is why it is important to include it when calculating the DOS of anatase.

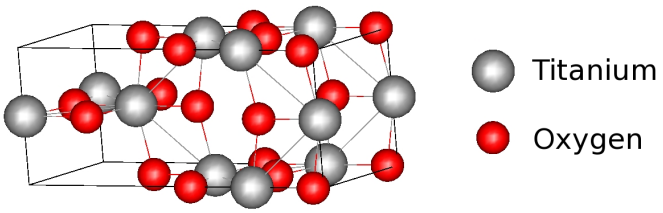

Figure 10 *– The anatase unit cell*

We performed Bader analysis to the all four calculations of the bulk anatase. The charges depend little on the number of $\vec{k}$-points and converge as the number increases. The oxygen atoms have an electronic charge of 9 e^- and the titanium atoms 20 e^-, with less than 0.1 e^- deviations (e^- being the charge of an electron). This indicates that in anatase the basic unit has formal charges of $Ti^{2+}O^-$.

We calculated the bulk anatase DOS also with the PBE+U functional. The results are shown in Figure 12. The PBE+U method is designed for

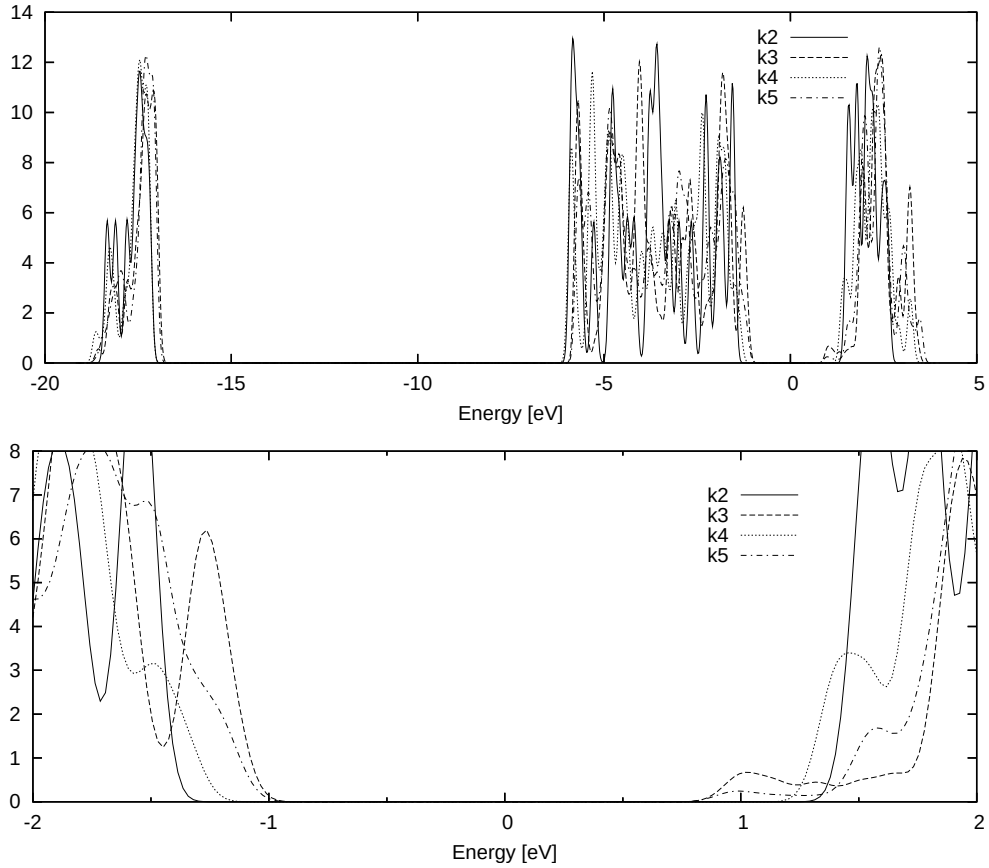

Figure 11 *– The density of states of the bulk anatase with different number of $\vec{k}$-points. The Fermi energy is shifted to zero.*

transition metal and it produces better band gap compared to the PBE. The band gaps are roughly $2.1\ \mathrm{eV}$ and $3.1\ \mathrm{eV}$ with the PBE and the PBE+U, respectively (here the band gap is defined as the energy difference of the highest energy of the VB and the lowest energy of the CB among all the $\vec{k}$-points used in calculation).

3.3 Anatase (101) surface

Spectroscopic experiments[32] suggest that in porous titanium dioxide the anatase (101) surface is one of the most exposed surfaces. It is then likely that large proportion of the attached dye molecules is attached onto this surface. Therefore we built our titanium dioxide models so that we can attach the dye molecules on the anatase (101) surface.

But what is anatase (101) surface? The digits (101) refer to the Miller

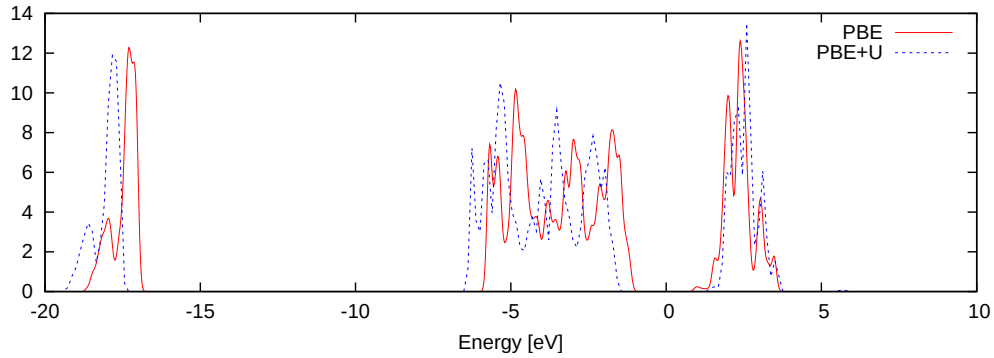

Figure 12 *– The bulk anatase DOS with the PBE and the PBE+U functionals*

indices, which define a cut plane in the unit cell. The unit cell[2] and this plane is shown in Figure 13a. When the bulk anatase is cut using this surface the emerging surface is called the anatase (101) surface.

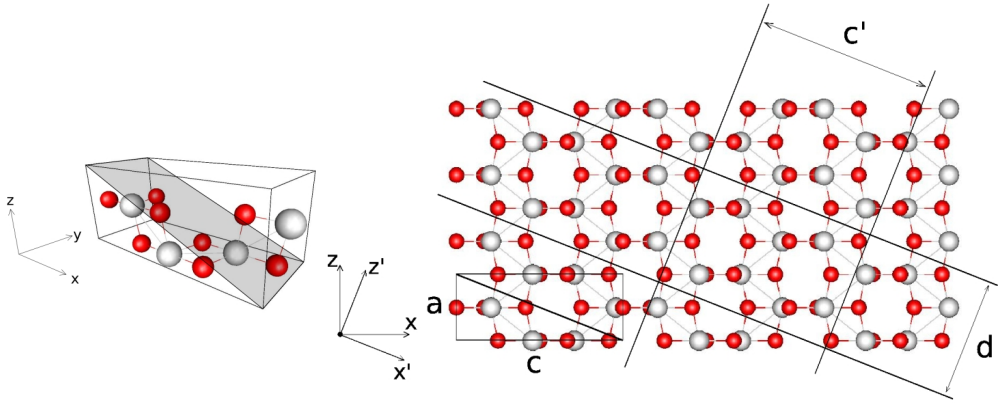

(a) anatase unit cell **(b)** anatase (101)-surface

Figure 13 *– Left: The unit cell of the anatase and the (101) plane cutting the cell. Right: The visualization of the anatase (101) surface in the bulk structure. The lines actually represent planes.*

In Figure 13b the unit cell is repeated in $\vec{x}$- and $\vec{z}$-directions to produce a bulk anatase particle. The cut plane is shown as a line from this direction and a two other (101) planes are also drawn. One can notice that the anatase is periodic also in the $\vec{x}'$-direction, and the length c' can be calculated with basic trigonometry. The $\vec{y}$-axis is not changed so in that direction the periodicity is the same as in the bulk structure. However, in the $\vec{z}'$-direction

[2]Some of the atoms that are only partially inside the unit cell in Figure 10 are removed to prevent the formation of duplicate atoms when the unit cell is repeated.

the periodicity may be broken, which is the case here (at least the length of the period is moderately larger than a or c'). We can, however, fix the length c' to produce the slab of a thickness we want. This slab is periodic in $\vec{x}'$ and $\vec{z}$ -directions and can be used in periodic calculations.

3.4 Periodic surface models

We built two periodic surface models with different thicknesses. The first one has two layers and the second one three layers of titanium atoms, see Figure 14. The titanium layers (where this naming arises) can be easier seen in the Figure 13b where there is two layers of titanium atoms between the two (101)-planes. The sizes of these simulation boxes are roughly $10 \times 4 \times 14$ Å^3 and $10 \times 4 \times 17$ Å^3, respectively. In $\vec{z}$-direction there is 4 Å of empty space between the surface and the edges of the simulation box in both models. The empirical formulas for these structures are $O_{16}Ti_8$ and $O_{24}Ti_{12}$.

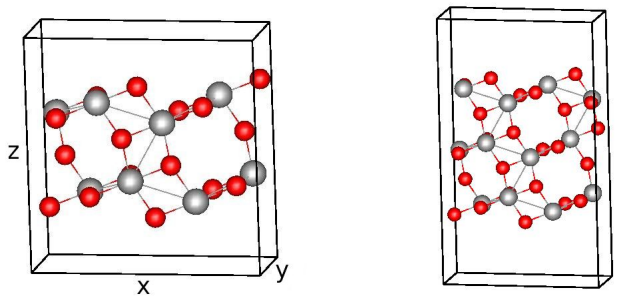

(a) 2-layer model **(b)** 3-layer model

Figure 14 *– The unit cells of the two periodic surface models. The cells can be repeated in x- and y- directions to simulate infinite surfaces of different thicknesses.*

We calculated the DOS for the 2-layer model with periocid boundary conditions in $\vec{x}$- and $\vec{y}$- directions and in all directions. Both calculations produced identical DOSs for the system. This tells that the empty space in the $\vec{z}$-direction is adequate and it is enough to apply the periodic directions only in x- and y-directions.

Then we calculated the DOS for the both surface models with another number of $\vec{k}$-points to see if that changes the DOS. The results are shown in Figure 15. There are very little differences within these calculations. The upper edge of the valence band is basically identical in all four calculations.

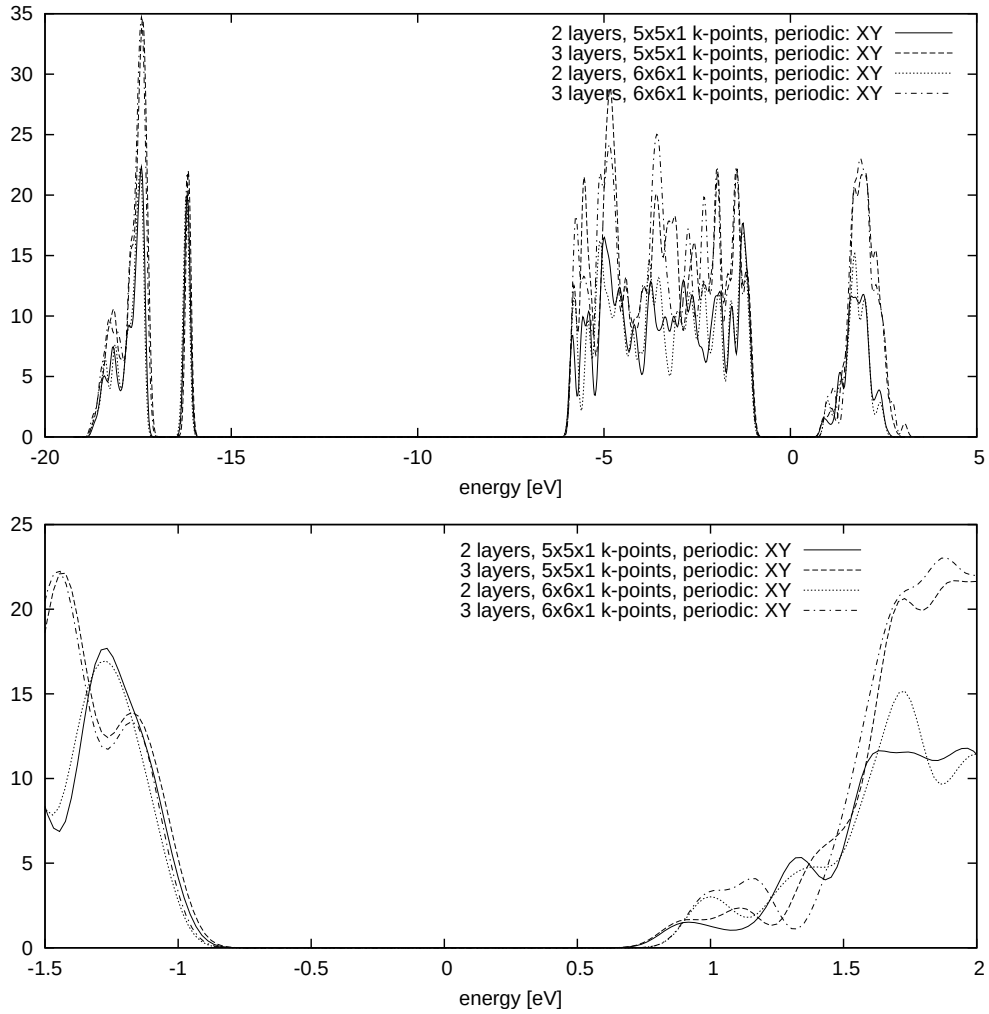

Figure 15 – *Density of states of the 2-layer and 3-layer model calculated with two different numbers of k-points. The Fermi energy is shifted to zero.*

The lower edge of the conduction band seems to be little bit dependent of the number of $\vec{k}$-points used in calculation. Again it is seen that the inclusion of the Γ-point results to a little bump at the edge of the conduction band.

When a nanoparticle of anatase is cut from a bulk anatase the atoms near the surface feel different potential than the atom deep inside the particle. This causes structural changes in the surface region. The effect weakens deeper in the particle and deep enough under the surface the structure is basically unaltered. In the 2-layer model we can think that

the unit cell consist of two layers of titanium and oxygen atoms that are separated by additional oxygens (the oxygens 6, 8, 10 and 17 in Figure 16). We optimized the structure of the 2-layer model partially so that we kept the lower layer and the separating oxygens fixed and let the upper layer relax. The unrelaxed and relaxed cells are plotted on top of each other in Figure 16. The density of states of the unrelaxed and relaxed structures are plotted in Figure 17. There were a different number of empty states in these two calculations which is why the tails differ at energies over $2\ \mathrm{eV}$.

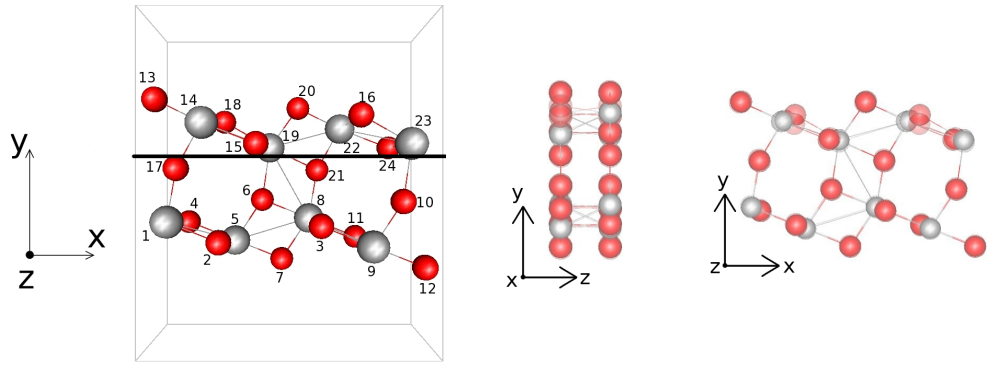

Figure 16 *– Left: The cell used in the Bader analysis. The line in the middle of the figure separates the atoms that were allowed to move (upper) and the atoms that were kept fixed (lower). Middle and right: The unrelaxed and relaxed structure plotted onto each other to visualize the movement.*

The overall shapes of these two DOSs are more or less equal. The relative weights differ at some energies, but the band gap region is basically unaltered by the relaxation.

The DOS of the bulk anatase and the relaxed 2-layer surface model are compared in Figure 18. In principle all the differences between these are due to the surface effects of the surface model. Compared to the bulk anatase the surface model has slightly more narrow band gap. Also the little bump at the edge of the CB in the bulk is more visible in the surface model. In the surface model there is one totally new state at $-16\ \mathrm{eV}$.

We performed Bader analysis to both relaxed and unrelaxed cells to see how the structure optimization affects the charges. The unit cell is shown in Figure 16 where the atoms are labeled. The cell is the same that is shown in Figure 14a, except that this time the surface atoms are allowed to relax. The relaxation affected strongest the oxygen atoms 16 and 18, which moved 0.43 Å away from the surface (the y-direction). Also the oxygen atoms 13 and 20 moved away from the surface but only 0.1 Å, and the oxygens 15 and 24 even less than that. The four titanium atoms that were

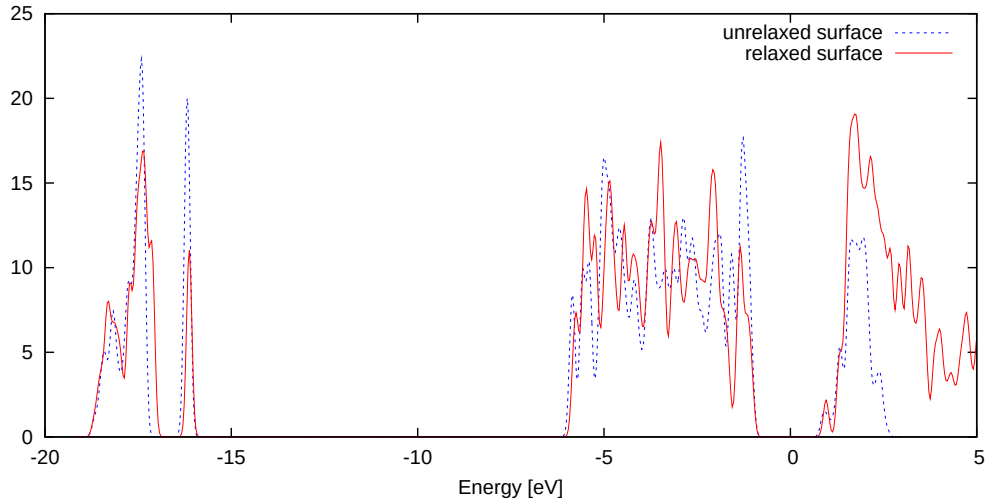

Figure 17 *– The density of states of the unrelaxed and partially relaxed 2-layer models.*

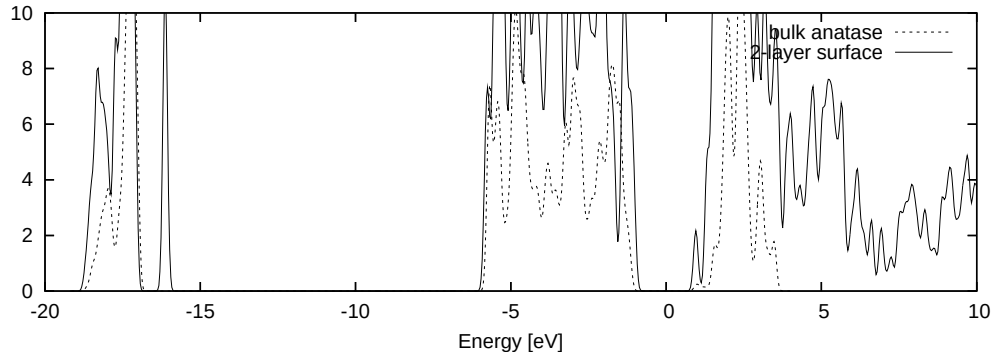

Figure 18 *– The DOS of the bulk anatase and the 2-layer surface model*

allowed to move shifted only about 0.17 Å each. Overall the relaxation of the surface-layer atoms did not cause substantial changes to the model and the charges changed less than 0.1 e^-.

The formal charges in both the bulk anatase and the surface model yield that the oxygens in anatase are in the anionic O^- form and the titanium atoms in cationic Ti^{2+} form. This is in agreement with results from Labat et al. [22] where they also calculated the charges of Ti and O to be close to +2 and -1, respectively. Especially in organic chemistry it is often assumed that oxygens in compounds are in the anionic O^{2-} form. This might be important

to keep in mind when trying to undestand the chemical reactions taking place on the surface of anatase surfaces.

We calculated the DOS with the PBE+U functional also for the surface model. The PBE and the PBE+U results are compared in Figure 19. The PBE+U again produces wider band gap compared to the PBE. The band gaps are $1.9\ \mathrm{eV}$ and $2.7\ \mathrm{eV}$, respectively.

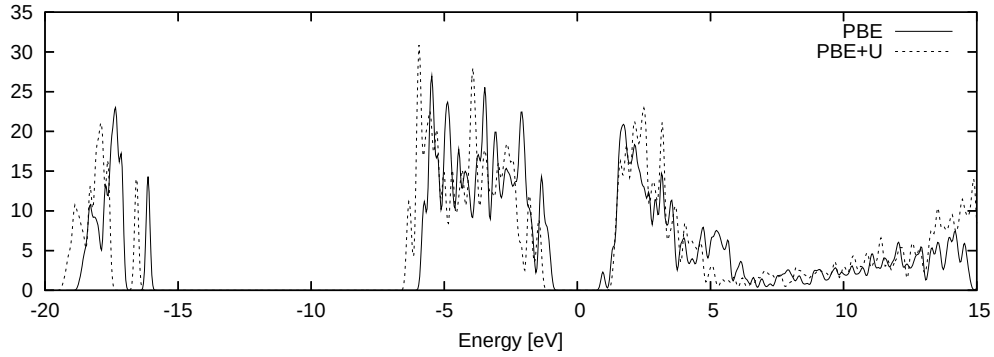

Figure 19 *– The DOS of the 2-layer surface model calculated with the PBE and the PBE+U functional.*

3.5 Cluster model

We also have a cluster model to describe the anatase (101) surface. Cluster model means that is is not periodic, and the calculations are performed in the same way as for the dye molecules in vacuum. This model is shown in Figure 20. The cluster model can be built by cutting a suitable piece from the surface of the anatase (101) surface. Cutting the covalent bonds leaves unsaturated bonds at the surfaces of the cluster. These dangling bonds are usually passivated by attaching hydrogens on them. We chose the number of hydrogens so that the cluster can be thought to consist of water and titanium dioxide molecules. The empirical formula of this model is then $(H_2O)_8 \cdot (TiO_2)_9 = H_{16}O_{26}Ti_9$.

The DOSs calculated using the PBE, PBE0 and PBE+U functionals are shown in Figure 21. Unfortunately there are only few empty states in the PBE0 calculation and the conduction band resembles more a single state than a band. When compared to the PBE calculations the PBE0 gives wider band gap, which is consistent with previous results. The PBE+U does not substantially change the DOS. The PBE+U should only affect the titanium atoms, and in this model less than 20% are Ti-atoms, compared to the 33%

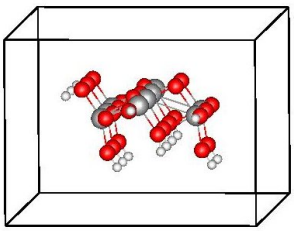

Figure 20 *– The cluster model in the simulation box. The empty space between the walls of the box is* 3 *Å.*

in the periodic model. This explains the small difference between the PBE and the PBE+U results.

The problem with trying to describe infinite structure with a finite small particle is that the band structure might be poorly developed. This leads to the situation that the cluster does not describe well the qualities of the infinite structure (the nanoparticles existing for example in the Grätzel cells can be considered infinite in the atomic scale). We can test this by comparing the density of states of the cluster model and the periodic surface. This is done in Figure 22. From the figure one can see that the DOS of the periodic model is smoother than the DOS of the cluster model, which contains isolated peaks at energies where the periodic model has no states at all. This is due to the small size of this model. The band structure is not fully developed and single molecular orbital-like states are present. Also the band gap is slightly wider in the periodic model.

An interesting case is the peak at the top of the valence band of the cluster. This peak seems to be completely missing from the DOS of the periodic model. Further analysis revealed that the peak consists of two states. The Kohn-Sham wave functions of these states are shown in the Figure 23. These wave functions are located on the ”artificial” surface that does not exists in a real situation. This indicates that the cluster model has some difficulties describing the real nanoparticle. On the other hand these states are not localized on the surface where the dye molecule is going to be attached. It is possible that these states do not interact with the dye, leaving a chance to proceed with calculations and ignore the peak in the band gap.

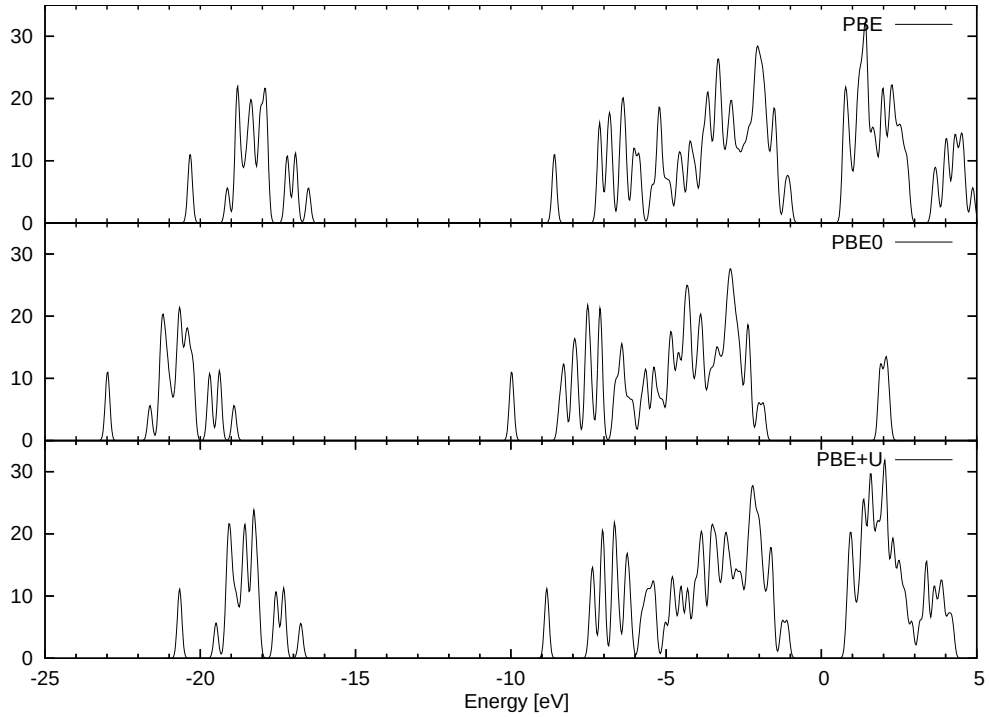

Figure 21 *– The DOS of the cluster model calculated with the PBE, PBE0 and PBE+U functionals.*

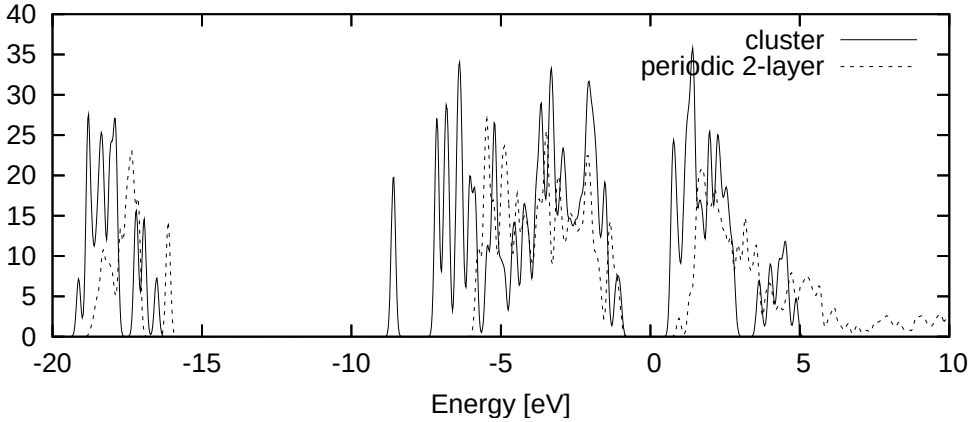

Figure 22 *– The density of states of the cluster model and the partially relaxed 2-layer periodic model*

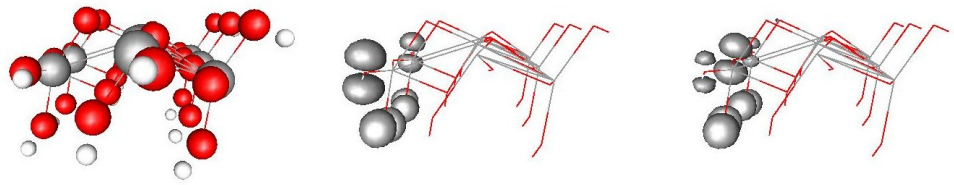

Figure 23 *– The cluster model and the two states that are isolated from the valence band.*

3.6 Cluster model with nko_001

We attached the dye molecule from the COOH-group to two titanium atoms on the anatase (101) surface. We added 3 Å of empty space between the atoms and the edges of the simulation cell. The structure was then relaxed so that the dye molecule, the two titanium atoms and the oxygen atom between them was allowed to move while the rest of the atoms were kept fixed. The relaxation was performed using the PBE functional. The relaxed structure is shown in Figure 24. The DOS is calculated using the PBE and the PBE+U functionals. The results are shown in Figure 25.

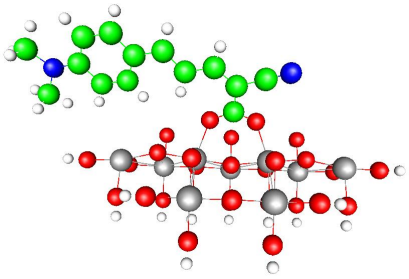

Figure 24 *– The cluster model with dye molecule nko_001.*

In both calculations the HOMO is located at the edge of the valence band and all the occupied states are basically identical in both calculations. In the PBE PDOS the LUMO is located almost inside the CB. The PBE+U shifts the CB up in energy but leaves the LUMO intact, and therefore in the PBE+U PDOS the LUMO is located in the band gap. These results are consistent with the bulk anatase calculation, where the PBE+U also widens the band gap. Unfortunately we were not able to perform the PBE0 calculations for this system.

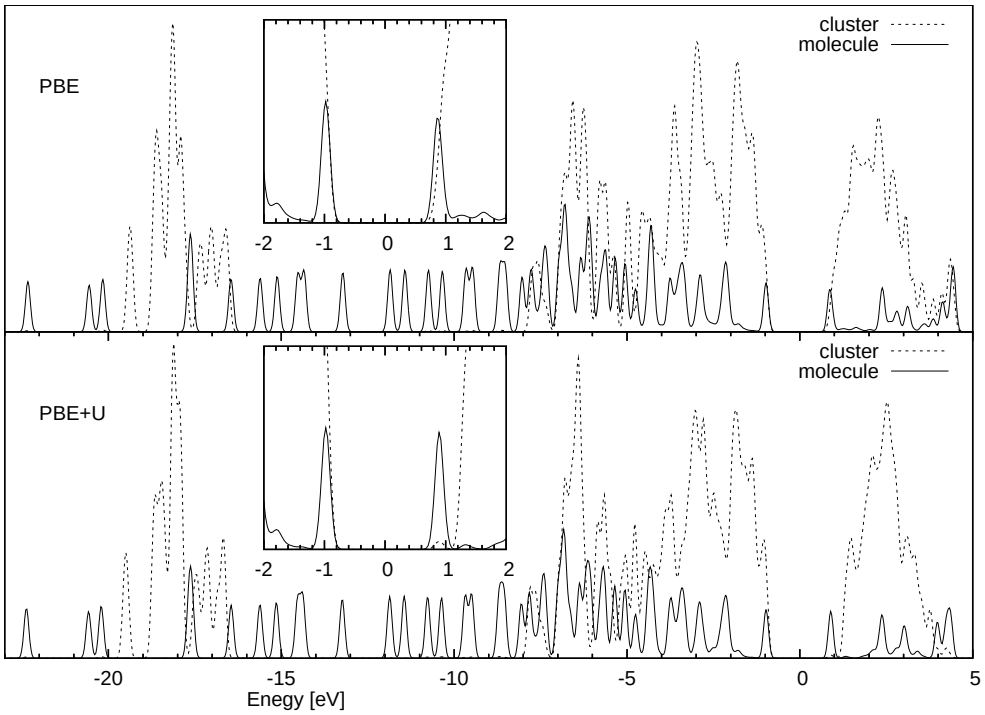

Figure 25 *– The PDOS of the cluster model with a dye molecule nko_001 calculated using the PBE and the PBE+U functionals.*

The molecular states from both calculations are plotted with sharper Gaussian peaks in Figure 26. Also the graphs with Gaussian peaks of 0.1 eV width are shown. In both calculations the HOMO looks like one state, due to the Gaussian broadening. Actually it consists of two states that are very close in energy. The wave functions of these states are shown in Figure 27. It can be seen that the artificial surface states do interact with the molecule HOMO states. The peak discussed in previous chapter is shifted closer to the valence band. This indicates that this model cannot describe the valence band-HOMO -region well. In the PBE calculation the LUMO has split into two states. This indicates that there is minor interaction between the LUMO and the CB. In the PBE+U calculation, where the LUMO is located in the band gap, there is no splitting.

Neither of the calculations are in good agreement with the general idea of the photoexcitation and the electron injection process represented in the Figure 1.2. The HOMO is expected to lie in the band gap and the LUMO inside the CB to make the photoexcitation possible. On the other hand, same kinds of results were obtained in a study performed by Duncan

et al. [8] (see Figure 28). Also in their calculations the LUMO is little below the conduction band. However, they predict that the HOMO is in the band gap. This is in disagreement with our calculations with sensitized cluster calculations.

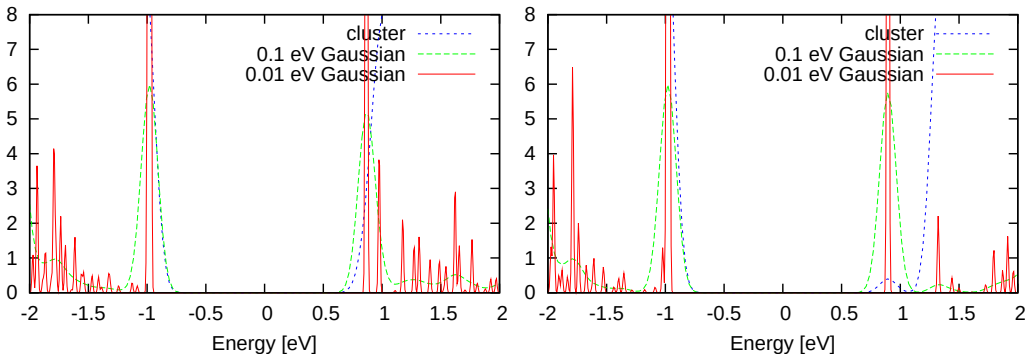

Figure 26 *– The broadening of the LUMO in the cluster model with dye nko_001. Left: the PBE calculation. Right: the PBE+U calculation.*

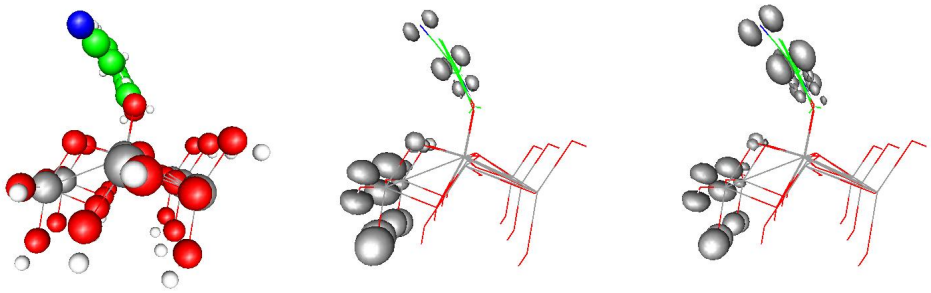

Figure 27 *– The KS-states of the two highest occupied states of the sensitized cluster model*

3.7 Periodic model with nko_001

Attaching the dye molecule onto the periodic model is slightly more problematic because we cannot simply add empty space around the unit cell. Instead, we must first make a larger unit cell by taking integer multiples of the relaxed unit cell and glueing these together in the $\vec{x}$- and $\vec{y}$- directions. The new unit cell must be so large that the dye molecule fits easily on

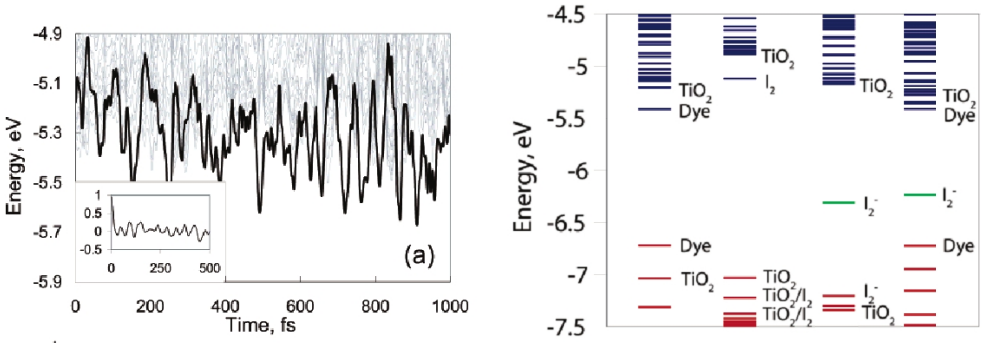

Figure 28 *– Left: The evolution of the photoexcited state (black) and the conduction band (grey) calculated in the ref. 8. Right: The energy states of a titanium dioxide with alizarin-molecule and an electrolyte molecule calculated in ref. 33.*

the surface. In addition there must be enough empty space between the molecule and the walls of the simulation cell to prevent unwanted interaction between the dye and its duplicates in adjacent cells. We constructed such a cell by repeating the relaxed 2-layer structure (Figure 14a) five times in the $\vec{y}$-direction. This, with the attached dye molecule, is shown in Figure 29. The empirical formula of the surface+dye is $(O_{80}Ti_{40})+(H_{13}C_{14}N_2O_2)$

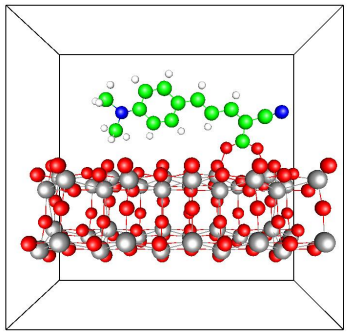

Figure 29 *– The periodic surface model with nko_001 in the simulation box*

The relaxation of this structure was performed in the same way as we relaxed the periodic surface model. The lower layer and the separating oxygens between the two layers were kept fixed and all the rest of the atoms were allowed to move. Since the titanium surface model is now five time larger than in the surface-only calculation there were also five times more surface atoms that needed to be relaxed. The PBE functional was

used in the relaxation calculations.

The PDOS of the relaxed system is calculated using the PBE and the PBE+U functionals, shown in Figure 30. The occupied states are basically identical in these calculations. In both the HOMO is located in the band gap, and not inside the valence band. This is in agreement with the results obtained by Duncan et al. [8] The differences between the PBE and the PBE+U are seen in the location of the conduction band. With PBE the LUMO can be considered to lie inside the CB. The PBE+U lifts the CB up in energy but does not affect the molecular states, and therefore the LUMO is in the band gap in the PBE+U calculation.

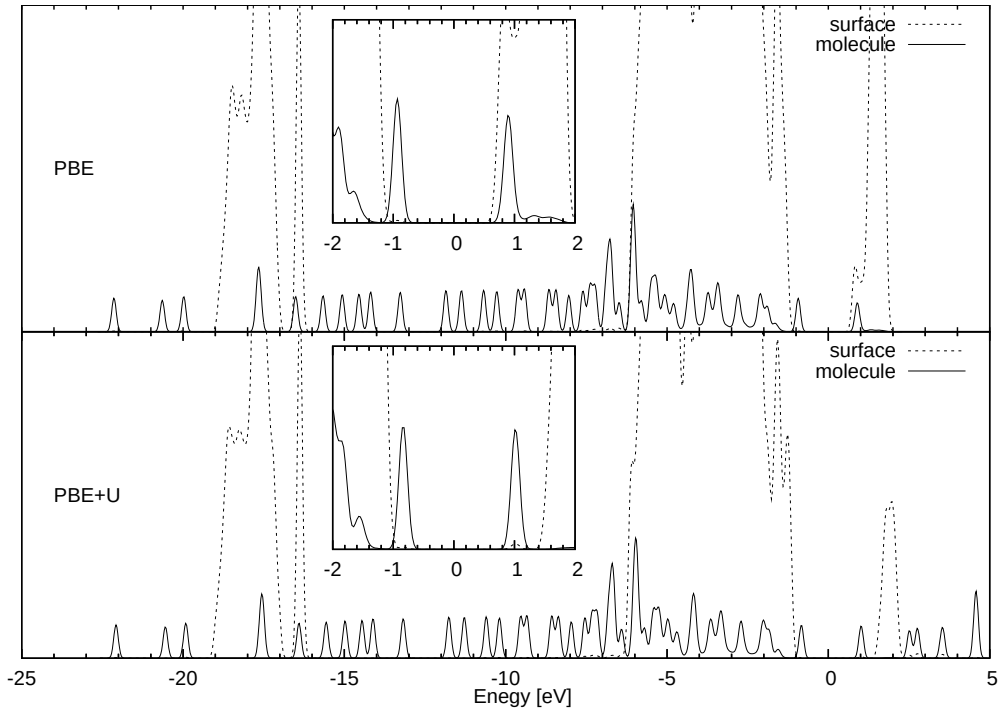

Figure 30 *– The PDOS of the periodic model with the nko_001 attached calculated using the PBE and the PBE+U functionals.*

The molecule PDOSs with sharper Gaussians are shown in Figure 31. The HOMO in both calculations is in the band gap and is not broadened at all. In the PBE calculation the LUMO is located inside the CB and minor broadening can be seen. Compared to the highest peak the broadening is very minimal. In the PBE+U the LUMO is in the band gap and no broadening is observed.

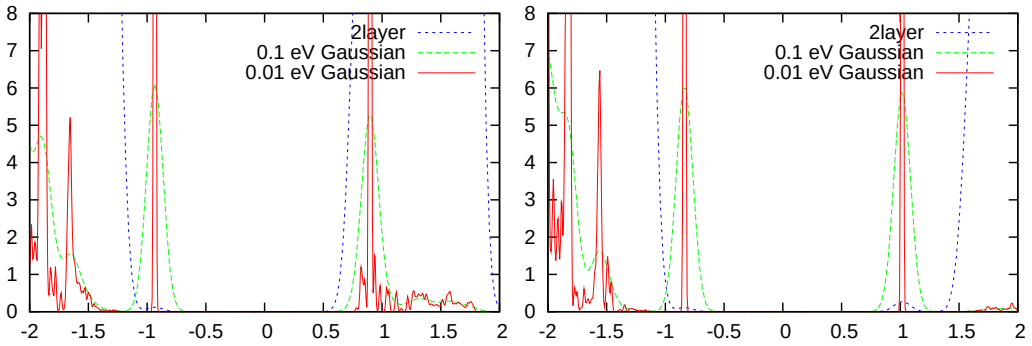

Figure 31 *– The broadening of the molecule states in the periodic model. Left: the PBE calculation. Right: the PBE+U calculation.*

3.8 Periodic model with perylene

Due to the standing alignment of the perylene on the surface, for this structure we needed to repeat the 2-layer model only four times to get suitable surface model, shown in Figure 32. The empirical formula is $(O_{64}Ti_{32})+(H_{11}C_{21}O_2)$. The relaxation was also done so that the atoms in the lower layer and the separating oxygens were kept fixed and all the others were allowed to relax.

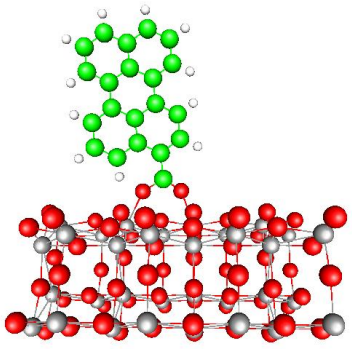

Figure 32 *– The periodic surface with perylene*

The PDOS is shown in Figure 33. The HOMO is located in the band gap also in this calculation but the LUMO is below the edge of the CB. Again, this is in agreement with the results in ref. 8.

Compared to another study from Persson et al. [7] the results are totally different. They studied perylene on large titanium dioxide cluster model

and predicted that the HOMO is located clearly in the band gap and the LUMO inside the conduction band (see Figure 34). The even developed a method to predict the electron-transfer time from the LUMO to the conduction band. The differences to our study is that they used a cluster model instead of a periodic surface and an exchange-correlation functional called B3LYP.[34,35] The surface model should not affect the results so much that it alone could explain the differences, since our calculations with nko_001 using cluster and periodic surface models were consistent with each other. The B3LYP has exact exchange mixed in it so that resembles the PBE0 we used to calculate the DOS of the cluster model. The PBE0 calculations were clearly different from the PBE and PBE+U calculations, so the different functional could explain the differences between our calculations and the ones in ref. 7. Labat et al. [22] calculated band gaps for rutile and anatase with several XC functionals, including PBE, PBE0 and B3LYP. The PBE underestimates the gap and B3LYP and PBE0 overestimate it, PBE0 even more than B3LYP. This also supports the conclusion that this kind of system is very dependent on the used XC functional.

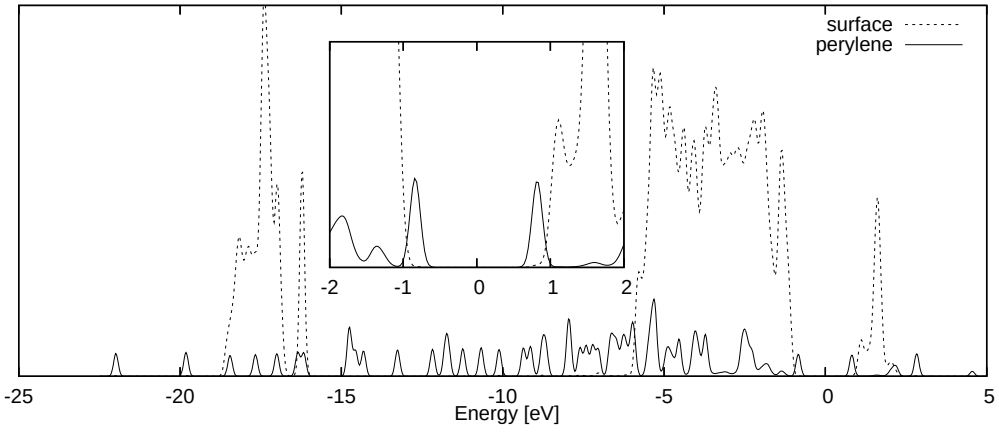

Figure 33 *– The PDOS of the 2-layer periodic surface model with perylene using the PBE functional*

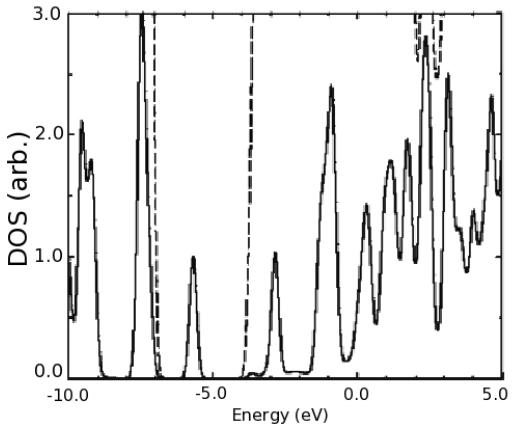

Figure 34 *– The PDOS of a perylene on titanium dioxide calculated by Persson et al.[7] Solid line = the perylene and the anchor groups, dash-dotted line = titanium dioxide PDOS. The HOMO of the perylene is in the band gap and the LUMO well inside the conduction band.*

4 Conclusions

In this work we have studied the interaction of dye molecules and titanium dioxide surface using density functional theory. We used two different dye molecules and two essentially different surface models to describe TiO_2 nanoparticles.

The comparison of the density of states of the surface models revealed that the cluster model introduces molecule-like single states that do not appear in the periodic surface model. The band structure is little poorly developed and the band gap is more narrow than in the periodic model. This is expected since the cluster model is, in fact, a large TiO_2 molecule. The artificial surfaces in the cluster model introduce unphysical states to the band gap region of the DOS. The periodic model produces a smoother DOS and does not substantially differ from the DOS calculated for the bulk anatase. Both models still offer a good description of the TiO_2 nanoparticle. The periocid model is physically more correct but the cluster model is computationally easier to handle.

The PDOS of the sensitized cluster model does not support the idea represented in the section 1.2. The PBE calculations predict that the HOMO is inside the valence band and the LUMO on the edge of the conduction band. The LUMO can be thought to consists of two states, so minor interaction between the LUMO and the CB can be observed. Changing to the PBE+U functional shifts the conduction band upwards in energy, leaving

the LUMO in the band gap and removing the interaction.

In the PDOS of the sensitized periodic model the HOMO is located in the band gap and the LUMO is located inside the conduction band. The differences to the PDOS of the cluster model are not huge in energy but qualitatively different, and the periodic model predicts that the states are located more like in the initial picture. In the PBE calculation the LUMO is slightly broadened compared to the vacuum calculations which means that we see weak interaction between the LUMO and the CB. The same kind of situation was considered in ref. 8 where they studied alizarin dye molecule attached on a titanium dioxide nanoparticle. Their study also revealed that the LUMO was located at the edge of the conduction band. However, they applied molecular dynamics (heat vibrations) to the system. They predict that the movement of the atoms causes fluctuations to the energy levels. According to their calculations the LUMO would be located in the conduction band some of the time, making the electron injection process described in section 1.2 possible. Unfortunately we can not see this in out zero temperature time-independent calculations. Compared to the PBE the PBE+U moves the CB upwards in energy and separated the LUMO and the CB, thus removing the interaction.

The PBE+U has the same effect in the cluster and in the periodic model: the conduction band moves up in energy relative to the VB and the molecule states. Compared to the PBE, the calculations with the PBE+U give results that are less in agreement with the initial picture of the photoexcitation process.

Changing the dye from nko_001 to perylene in the periodic model does not substantially affect the PDOS of the system. The HOMO is located in the band gap and the LUMO at the edge of the CB in both systems.

Our results are in good agreement with another similar study performed by Duncan et al. [33]. They also got results indicating that the HOMO and the LUMO are located near the edges of the valence and conduction band, respectively. They used time-dependent DFT and the exchange-correlation functional PW91 which is close to the PBE.

Persson et al. [7] have made a similar study with large TiO_2 cluster model and perylene dye molecule. In their study the HOMO settles clearly in the band gap and the LUMO inside the CB. The most significant difference between their study and ours is the used XC-functional. They used the functional called B3LYP, whereas we used the PBE and the PBE+U. We can conclude that the XC-functional has an unpleasantly large effect to the results in this kind of system. The calculations with the PBE0 functional might be better in agreement with the results from Persson et al. and also with the general idea of electron injection process in the DSCs.

More investigation is needed in order to use simulation results to find optimal dye molecules for the DSCs. The interpretation of the location of the states is not clear and the used exchange-correlation functional must be taken into account.

References

[1] Photovoltaics: Solar Electricity and Solar Cells in Theory and Practice. `www.solarserver.de/wissen/photovoltaik-e.html`, 04 2008.

[2] Martin A. Green. High Efficiency Silicon Solar Cells. Technical report, University of New South Wales, Photovoltaics Special Research Centre, Sydney, Australia, 2052, 1997.

[3] A. Hagfeldt and M. Grätzel. Molecular photovoltaics. *Acc. Chem. Res.*, 33(5):269–277, 2000.

[4] Nick Vlachopoulos, Paul Liska, Jan Augustynski, and Michael Grätzel. Very Efficient Visible Light Energy Harvesting and Conversion by Spectral Sensitization of High Surface Area Polycrystalline Titanium Dioxide Films. *Journal of American Chemical Society*, 110:1216–1220, 1988.

[5] S. R. Elliot. *The Physics and Chemistry of Solids*. John Wiley & Sons, 2006. ISBN 0-471-98195-8.

[6] Takayuki Kitamura, Masaaki Ikeda, Koichiro Shigaki, Teruhisa Inoue, Neil A. Anderson, Xin Ai, Tianquan Lian, and Shozo Yanagida. Phenyl-Conjugated Oligoene Sensitizers for TiO_2 Solar Cells. *Chemistry of Materials*, 16:1806–1812, 2004.

[7] P. Persson, M. J. Lundqvist, R. Ernstorfer, W. A. Goddard III, and F. Willig. Quantum Chemical Calculations of the Influence of Anchor-Cum-Spacer Groups on Femtosecond Electron Transfer Times in Dye-Sensitized Semiconductor Nanocrystals. *Journal of Chemical Theory and Computation*, 2:441–451, 2006.

[8] Walter R. Duncan, William M. Stier, and Oleg V. Prezhdo. Ab Initio Nonadiabatic Molecular Dynamics of the Ultrafast Electron Injection across the Alizarin-TiO_2 Interface. *Journal of American Chemical Society*, 127:7941–7951, 2005.

[9] Liisa Antila. Varauksenkuljetus ja rekombinaatioreaktiot väriaineaurinkokennon aktiivisella elektrodilla. Master's thesis, University of Jyväskylä, Department of Chemistry, 2006.

[10] Anders Hagfeldt and Michael Grätzel. Light-Induced Redox Reactions in Nanocrystalline Systems. *Chemical Reviews*, 95:49–68, 1995.

[11] Robert N. Barnett and Uzi Landman. Born-Oppenheimer molecular-dynamics simulations of finite systems: Structure and dynamics of $(H_2O)_2$. *Physical review B*, 48(4), 1993.

[12] Robert G. Parr and Weitao Yang. *Density-Functional Theory of Atoms and Molecules*. Oxford University Press, 1989.

[13] P. Hohenberg and W. Kohn. Inhomogenous Electron Gas. *Physical Review*, 136(3B), 1964.

[14] W. Kohn and L. J. Sham. Self-Consistent Equations Including Exchange and Correlation Effects. *Physival Review*, 140(4A), 1965.

[15] K. Burke, J Werschnik, and E.K.U. Gross. Time-dependent density functional theory: Past, present, and future. *The Journal of Chemical Physics*, 123:062206, 2005.

[16] John P. Perdew and Yue Wang. Accurate and simple analytic representation of the electron-gas correlation energy. *Physical Review B*, 45(23), 1992.

[17] John P. Perdew, Kieron Burke, and Matthias Ernzerhof. Generalized Gradient Approximation Made Simple. *Physical Review Letters*, 77(18): 3865–3868, 1996.

[18] J. P. Perdew. *Structure of solids '91*. Akademie Verlag, Berlin, 1991. edited by P. Ziesche and H. Eschrig.

[19] John P. Perdew, Matthias Ernzerhof, and Kieron Burke. Rationale for mixing exact exchange with density functional approximations. *Journal of Chemical Physics*, 105(22), 1996.

[20] Carlo Adamo and Vincenzo Barone. Towards a reliable density funtional methods without adjustable parameters: The PBE0 model. *Journal of Chemical Physics*, 110(13), 1999.

[21] Vladimir I Anisimov, F Aryasetiawan, and A I Lichtenstein. First-principles calculations of the electronic structure and spectra of strongly correlated systems: the LDA+U method. *Journal of Physics: Condensed Matter*, 9:767–808, 1997.

[22] Frèderic Labat, Philippe Baranek, Christophe Domain, Christian Minot, and Carlo Adamo. Density functional theory analysis of the structural and electronic properties of TiO_2 rutile and anatase polytypes: Performances of different exchange-correlation functionals. *The Journal of Chemical Physics*, 126(154703), 2007.

[23] P. E. Blöchl. Projector augmented-wave method. *Physical Review B*, 50 (24), 1994.

[24] J. J. Mortensen, L. B. Hansen, and K. W. Jacobsen. Real-space grid implementation of the projector augmented wave method. *Physical Review B*, 71(035109), 2005.

[25] Grid-based projector-augmented wave method. `https://wiki.fysik.dtu.dk/gpaw/GPAW`, 04 2008.

[26] WebElements. `www.webelements.com/`, 04 2008.

[27] Graeme Henkelman, Andri Arnaldsson, and Hannes Jonsson. A fast and robust algorithm for bader decomposition of charge density. *Computational Material Science*, 36:354–360, 2006.

[28] N. Troullier and J. L. Martins. Efficient pseudopotentials for plane-wave calculations. *Physical Review B*, 43(3), 1991.

[29] Pavan K. Naicker, Peter T. Cummings, Hengzhong Zhang, and Jillian F. Banfield. Characterization of Titanium Dioxide Nanoparticles Using Molecular Dynamics Simulations. *Journal of Physical Chemistry B*, 109: 15243–15249, 2005.

[30] R. Asahi, Y. Taga, W. Mannstadt, and A. J. Freeman. Electronic and optical properties of anatase TiO_2. *Physical Review B*, 61(11), 2000.

[31] A. Beltran, J. R. Sambrano, M. Calatayud, F. R. Sensato, and J: Andres. Static simulation of bulk and selected surfaces of anatase TiO_2. *Surface Science*, 490:116–124, 2001.

[32] Christophe J. Barbe, Francine Arendse, Pascal Comte, Marie Jirousek, Frank Lenzmann, Valery Shklover, and Michael Gratzel. Nanocrystalline Titanium Oxide Electrodes for Photovoltaic Applications. *J. Am. Ceram. Soc*, 80(12), 1997.

[33] Walter R. Duncan, Colleen F. Craig, and Oleg V. Prezhdo. Time-Domain ab Initio Study of Charge Relaxation and Recombination in Dye-Sensitized TiO_2. *Journal of American Chemical Society*, 129:8528–8543, 2007.

[34] K. Kim and K. D. Jordan. Comparison of Density Functional and MP2 Calculations on the Water Monomer and Dimer. *J. Phys. Chem.*, 98: 10089–10094, 1994.

[35] Chengteh Lee, Weitao Yang, and Robert G. Parr. Development of the Colle-Salvetti correlation-energy formula into a functional of the electron density. *Physical review B*, 37(2), 1988.

A Functional derivatives

The functional derivative can be defined as

$$\frac{\delta F[g(\vec{x})]}{\delta g(\vec{y})} = \lim_{\xi \to 0} \frac{F[g(\vec{x}) + \xi\delta(\vec{x} - \vec{y})] - F[g(\vec{x})]}{\xi} \tag{31}$$

From equations (3) and (4) one gets

$$E[n(\vec{r})] = T_S[n(\vec{r})] + \int n(\vec{r}) V_{ext}(\vec{r}) d\vec{r} + \frac{e^2}{2} \iint \frac{n(\vec{r}) n(\vec{r}\,')}{|\vec{r} - \vec{r}\,'|} d\vec{r} d\vec{r}\,' + E_{XC}[n(\vec{r})] \,. \tag{32}$$

Derivating the terms with integrals one gets

$$\begin{aligned}
&\frac{\delta}{\delta n(\vec{R})} \int n(\vec{r}) V_{ext}(\vec{r}) d\vec{r} \\
&\qquad = \lim_{\xi \to 0} \int \frac{\Big(n(\vec{r}) + \xi\delta(\vec{r} - \vec{R})\Big) V_{ext}(\vec{r}) - n(\vec{r}) V_{ext}(\vec{r})}{\xi} d\vec{r} \\
&\qquad = \lim_{\xi \to 0} \int \frac{\Big(\xi\delta(\vec{r} - \vec{R})\Big) V_{ext}(\vec{r})}{\xi} d\vec{r} \\
&\qquad = \int \delta(\vec{r} - \vec{R}) V_{ext}(\vec{r}) d\vec{r} = V_{ext}(\vec{R})
\end{aligned} \tag{33}$$

$$\begin{aligned}
&\frac{\delta}{\delta n(\vec{R})} \frac{e^2}{2} \iint \frac{n(\vec{r}) n(\vec{r}\,')}{|\vec{r} - \vec{r}\,'|} d\vec{r} d\vec{r}\,' \\
&\quad = \lim_{\xi \to 0} \frac{e^2}{2} \iint \frac{(n(\vec{r}) + \xi\delta(\vec{r} - \vec{R}))(n(\vec{r}\,') + \xi\delta(\vec{r}\,' - \vec{R})) - n(\vec{r}) n(\vec{r}\,')}{\xi |\vec{r} - \vec{r}\,'|} d\vec{r} d\vec{r}\,' \\
&\quad = \lim_{\xi \to 0} \frac{e^2}{2} \iint \frac{n(\vec{r})\xi\delta(\vec{r}\,' - \vec{R}) + n(\vec{r}\,')\xi\delta(\vec{r} - \vec{R})}{\xi |\vec{r} - \vec{r}\,'|} d\vec{r} d\vec{r}\,' \\
&\quad = \underbrace{\frac{e^2}{2} \iint \frac{n(\vec{r})\delta(\vec{r}\,' - \vec{R})}{|\vec{r} - \vec{r}\,'|} d\vec{r}\,' d\vec{r}}_{\text{integrate over } \vec{r}\,'} + \underbrace{\frac{e^2}{2} \iint \frac{n(\vec{r}\,')\delta(\vec{r} - \vec{R})}{|\vec{r} - \vec{r}\,'|} d\vec{r} d\vec{r}\,'}_{\text{integrate over } \vec{r}} \\
&\quad = \frac{e^2}{2} \int \frac{n(\vec{r})}{|\vec{r} - \vec{R}|} d\vec{r} + \frac{e^2}{2} \int \frac{n(\vec{r}\,')}{|\vec{r}\,' - \vec{R}|} d\vec{r}\,' \\
&\quad = e^2 \int \frac{n(\vec{r})}{|\vec{r} - \vec{R}|} d\vec{r}
\end{aligned} \tag{34}$$

B Bloch's theorem

The Fourier expansion of the periodic potential gives

$$V(\vec{r}) = \sum_{\vec{k}} \nu_{\vec{k}} e^{i\vec{k}\cdot\vec{r}}, \tag{35}$$

where the Fourier coefficients $\nu_{\vec{k}}$ are given by the Fourier transformation of the potential $V(\vec{r})$:

$$\nu_{\vec{k}} = \frac{1}{V_c} \int_{V_c} e^{-i\vec{k}\cdot\vec{r}} V(\vec{r}) d\vec{r}, \tag{36}$$

where V_c is the size of the unit cell. Using the equation (22) we get

$$V(\vec{r}) = \sum_{\vec{k}} \nu_{\vec{k}} e^{i\vec{k}\cdot\vec{r}} = \sum_{\vec{k}} \nu_{\vec{k}} e^{i\vec{k}\cdot(\vec{r}+\vec{R})} = \sum_{\vec{k}} \left(\nu_{\vec{k}} e^{i\vec{k}\cdot\vec{R}}\right) e^{i\vec{k}\cdot\vec{r}}. \tag{37}$$

This equation shows that $\vec{k}$-values in the sum must satisfy

$$\vec{k}\cdot\vec{R} = \pm 2\pi, \tag{38}$$

i.e, only the reciprocal lattice vectors must be included to the Fourier series of the periodic potential. These vectors are from now on denoted with a capital $\vec{G}$.

Also the wave function can be represented as a Fourier expansion

$$\Psi(\vec{r}) = \sum_{\vec{k}} c_{\vec{k}} e^{i\vec{k}\cdot\vec{r}}, \tag{39}$$

where the sum goes over all the $\vec{k}$-vectors in the reciprocal space and the coefficients defined again as

$$c_{\vec{k}} = \int_{V_c} e^{-i\vec{k}\cdot\vec{r}} \Psi(\vec{r}) d\vec{r} \tag{40}$$

With these definitions[5] we can express the Schrödinger equation as

$$\begin{aligned}
&\frac{\hbar^2 k^2}{2m}\Psi_{\vec{k}}(\vec{r}) + V(\vec{r})\Psi_{\vec{k}}(\vec{r}) = \epsilon\Psi_{\vec{k}}(\vec{r}) \\
\Rightarrow &\sum_{\vec{k}} \frac{\hbar^2 k^2}{2m} c_{\vec{k}} e^{i\vec{k}\cdot\vec{r}} + \left(\sum_{\vec{G}} \nu_{\vec{G}} e^{i\vec{G}\cdot\vec{r}}\right)\left(\sum_{\vec{k}} c_{\vec{k}} e^{i\vec{k}\cdot\vec{r}}\right) = \sum_{\vec{k}} \epsilon c_{\vec{k}} e^{i\vec{k}\cdot\vec{r}} \\
\Rightarrow &\sum_{\vec{k}} \frac{\hbar^2 k^2}{2m} c_{\vec{k}} e^{i\vec{k}\cdot\vec{r}} + \sum_{\vec{k}}\sum_{\vec{G}} c_{\vec{k}}\nu_{\vec{G}} e^{i(\vec{k}+\vec{G})\cdot\vec{r}} = \epsilon \sum_{\vec{k}} c_{\vec{k}} e^{i\vec{k}\cdot\vec{r}}
\end{aligned} \tag{41}$$

Now, making a change of a variable $\vec{k}' = \vec{k} + \vec{G}$, we get

$$\sum_{\vec{k}} \frac{\hbar^2 k^2}{2m} c_{\vec{k}} e^{i\vec{k}\cdot\vec{r}} + \sum_{\vec{k}'}\sum_{\vec{G}} c_{\vec{k}'-\vec{G}}\nu_{\vec{G}} e^{i\vec{k}'\cdot\vec{r}} = \epsilon \sum_{\vec{k}} c_{\vec{k}} e^{i\vec{k}\cdot\vec{r}} \tag{42}$$

In the middle term the $\vec{k}'$ is just a variable that goes over all the reciprocal vectors, so we can mark it with $\vec{k}$, and combine the exponential parts of the terms,

$$\sum_{\vec{k}} e^{i\vec{k}\cdot\vec{r}} \left[\frac{\hbar^2 k^2}{2m} + \sum_{\vec{G}} c_{\vec{k}-\vec{G}}\nu_{\vec{G}}\right] = \epsilon \sum_{\vec{k}} e^{i\vec{k}\cdot\vec{r}} c_{\vec{k}} \tag{43}$$

The coefficients of the Fouries expansions must be the same, so

$$\left(\frac{\hbar^2 k^2}{2m} - \epsilon\right) c_{\vec{k}} + \sum_{\vec{G}} \nu_{\vec{G}} c_{\vec{k}-\vec{G}} = 0 \tag{44}$$

The equation (44) is called the central equation. The differential equation in the real space has been turned into set of algebraic equations in the reciprocal space. From this equation we get a formula for the Fourier coefficients of the wave function:

$$c_{\vec{k}} = -\sum_{\vec{G}} \frac{\nu_{\vec{G}} c_{\vec{k}-\vec{G}}}{\frac{\hbar^2 k^2}{2m} - \epsilon} = \sum_{\vec{G}} \tilde{c}_{\vec{k}-\vec{G}}\nu_{\vec{G}}. \tag{45}$$

It can be seen that for a given $\vec{k}$ the coefficients $c_{\vec{k}}$ differ only by reciprocal lattice vectors. That means that the sum in the Fourier expansion of the wave function (39) needs to only cover the reciprocal lattice vectors instead

of all of them, viz.

$$\begin{aligned}\Psi(\vec{r}) &= \sum_{\vec{k}} c_{\vec{k}} e^{i\vec{k}\cdot\vec{r}} = \sum_{\vec{G}} c_{\vec{k}-\vec{G}} e^{i(\vec{k}-\vec{G})\cdot\vec{r}} \\ &= \left(\sum_{\vec{G}} c_{\vec{k}-\vec{G}} e^{-i\vec{G}\cdot\vec{r}} \right) e^{i\vec{k}\cdot\vec{r}} \\ &= e^{i\vec{k}\cdot\vec{r}} u_{\vec{k}}(\vec{r})\end{aligned} \tag{46}$$

If we now translate the wave function in the real space by a lattice vector $\vec{R}$, we get

$$\begin{aligned}\Psi_{\vec{k}}(\vec{r}+\vec{R}) &= e^{i\vec{k}\cdot(\vec{r}+\vec{R})} u_{\vec{k}}(\vec{r}+\vec{R}) \\ &= e^{i\vec{k}\cdot\vec{R}} e^{i\vec{k}\cdot\vec{r}} \sum_{\vec{G}} c_{\vec{k}-\vec{G}} e^{-i\vec{G}\cdot(\vec{r}+\vec{R})} \\ &= e^{i\vec{k}\cdot\vec{R}} \underbrace{e^{i\vec{k}\cdot\vec{r}} \sum_{\vec{G}} c_{\vec{k}-\vec{G}} e^{-i\vec{G}\cdot\vec{r}}}_{=\Psi_{\vec{k}}(\vec{r})} \underbrace{e^{-i\vec{G}\cdot\vec{R}}}_{=1} \\ &= e^{i\vec{k}\cdot\vec{R}} \Psi_{\vec{k}}(\vec{r}),\end{aligned} \tag{47}$$

where $\vec{G}\cdot\vec{R} = 2\pi$ by the definition of the reciprocal lattice. This is called the Bloch wave function. It can be seen that the electron wave functions in the periocic potential are periodic functions that are modulated by the exponential part. One should notice that the Bloch wave function is not periodic in the real space, see Figure 35.

The same kind of translation can be made in the reciprocal lattice with a reciprocal lattice vector $\vec{G}$:

$$\begin{aligned}\Psi_{\vec{k}+\vec{G}}(\vec{r}) &= e^{i(\vec{k}+\vec{G})\cdot\vec{r}} \sum_{\vec{G}'} c_{(\vec{k}+\vec{G})-\vec{G}'} e^{-i\vec{G}'\cdot\vec{r}} \\ &= \sum_{\vec{G}'} e^{i(\vec{k}+\vec{G}-\vec{G}')\cdot\vec{r}} c_{\vec{k}+\vec{G}-\vec{G}'} \\ &= \sum_{\vec{G}''} e^{i(\vec{k}-\vec{G}'')} c_{\vec{k}-\vec{G}''} \\ &= \Psi_{\vec{k}}(\vec{r}),\end{aligned} \tag{48}$$

where we used the change of a variable $-\vec{G}'' = \vec{G} - \vec{G}'$ which is allowed

since the sum of two (reciprocal) lattice vectors is also a lattice vector and the sum just goes over all the lattice vectors. This shows that the Bloch wave functions are periodic in the reciprocal lattice.

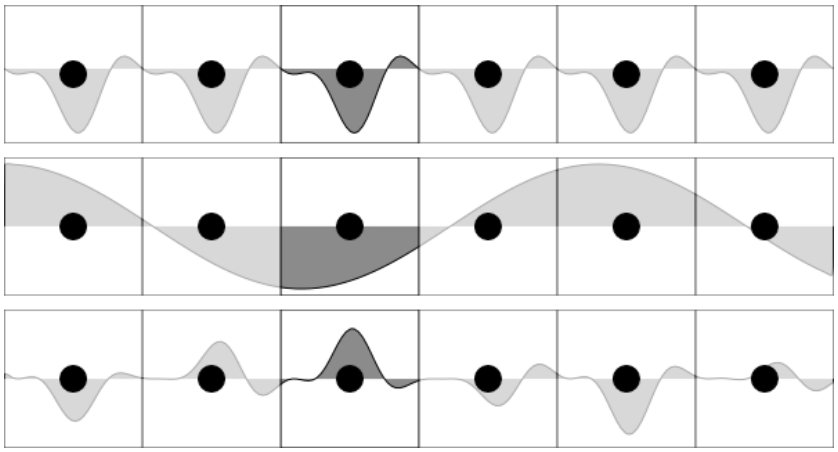

Figure 35 *– An one-dimensional example of a Bloch wave in the periodic simulation. The upper function $u_{\vec{k}}(\vec{r})$ has a periodicity of the real space lattice. In the middle the plane wave part $e^{i\vec{k}\cdot\vec{r}}$ has longer wave lenght than the lattice constant. The lowest is the total Bloch wave $\Psi_{\vec{k}}(\vec{r}) = e^{i\vec{k}\cdot\vec{r}}u_{\vec{k}}(\vec{r})$. The simulation box is drawn with darker colour. Note that this is just an example rather than a real wave function from the calculations.*